Direct measurement of N_2O_5 heterogeneous uptake coefficients on ambient aerosols via an aerosol flow tube system: design, characterization and performance

Xiaorui Chen[1,a], Haichao Wang[3,4*], Tianyu Zhai[1], Chunmeng Li[1], Keding Lu[1,2*]

[1]State Key Joint Laboratory of Environmental Simulation and Pollution Control, College of Environmental Sciences and Engineering, Peking University, Beijing, China.

[2]The State Environmental Protection Key Laboratory of Atmospheric Ozone Pollution Control, College of Environmental Sciences and Engineering, Peking University, Beijing, China

[3]School of Atmospheric Sciences, Sun Yat-sen University, Zhuhai, 519082, China

[4]Guangdong Provincial Observation and Research Station for Climate Environment and Air Quality Change in the Pearl River Estuary, Key Laboratory of Tropical Atmosphere-Ocean System, Ministry of Education, Southern Marine Science and Engineering Guangdong Laboratory (Zhuhai), Zhuhai, 519082, China

[a]now at: Department of Civil and Environmental Engineering, The Hong Kong Polytechnic University, Hong Kong, China

Correspondence to: Haichao Wang (wanghch27@mail.sysu.edu.cn), Keding Lu (k.lu@pku.edu.cn)

Abstract. An improved aerosol flow tube system coupled with detailed box model was developed to measure N_2O_5 heterogeneous uptake coefficients ($\gamma(N_2O_5)$) on ambient aerosols directly. This system features sequential measurements of N_2O_5 concentration at the both entrance and exit of the flow tube to ensure an accurate retrieval of N_2O_5 loss in the flow tube. Simulation and laboratory tests demonstrate that this flow tube system is able to overcome the interference from side reactions led by varying reactants (e.g., NO_2, O_3 and NO) and improve the robustness of results with the assistance of box model method. Factors related to $\gamma(N_2O_5)$ derivation were extensively characterized, including particle transmission efficiency, mean residence time in the flow tube and wall loss coefficient of N_2O_5, for normal operating

28 condition. The measured $\gamma(N_2O_5)$ on $(NH_4)_2SO_4$ model aerosols were in good agreement with

29 literature values over a range of relative humidity (RH). The detection limit of $\gamma(N_2O_5)$ was

30 estimated to be 0.0016 at low aerosol surface concentration (Sa) condition of 200 μm^2 cm^{-3}.

31 Given the instrument uncertainties and potential fluctuation of air mass between successive

32 sampling modes, we estimate the overall uncertainty of $\gamma(N_2O_5)$ that ranges from 16 to 43%

33 for different ambient conditions. This flow tube system was then successfully deployed for

34 field observations at an urban site of Beijing influenced by anthropogenic emissions. The

35 performance in field observation demonstrates that the current setup of this system is capable

36 of obtaining robust $\gamma(N_2O_5)$ amid the switch of air mass.

1 Introduction

38 Dinitrogen pentoxide (N_2O_5), forming from the reaction of nitrogen dioxide (NO_2) and nitrate

39 radical (NO_3), acts as an important reservoir of atmospheric nitrogen. The N_2O_5 can undergo

40 either thermal dissociation (back to NO_2 and NO_3; photolysis of NO_3 also generate NO_2) to

41 release NO_2 or hydrolysis (both homogeneous and heterogeneous) to remove nitrogen oxides

42 from the atmosphere (Brown and Stutz, 2012;Chang et al., 2011). Among the budgets of N_2O_5,

43 the uptake on aerosol particles is a highly efficient pathway to be responsible for production

44 of nitrate aerosol in some regions (Fu et al., 2020;Wang et al., 2019;Wang et al.,

45 2017c;Baasandorj et al., 2017;McDuffie et al., 2019;Prabhakar et al., 2017;Wang et al.,

46 2018a;Chen et al., 2020) and promote activation of chlorine via $ClNO_2$ formation (Bertram

47 and Thornton, 2009a;Osthoff et al., 2008;Tham et al., 2018;Thornton et al., 2010;Wang et al.,

48 2017f;Riedel et al., 2012a;Riedel et al., 2013;Gaston and Thornton, 2016;Mitroo et al., 2019).

49 The N_2O_5 uptake coefficient ($\gamma(N_2O_5)$) is critical in determining the uptake reaction rate of

50 N_2O_5 on aerosol in addition to aerosol surface area (Sa). It represents the fraction of collisions

51 between gaseous N_2O_5 molecules and particle surfaces that resulted in a loss of N_2O_5. Model

52 simulation showed the variations in $\gamma(N_2O_5)$ can significantly influence the fate of NOx, O_3

53 and OH radical in a regional (Li et al., 2016;Sarwar et al., 2012;Lowe et al., 2015) and global

54 scale (Dentener and Crutzen, 1993;Evans and Jacob, 2005;Macintyre and Evans, 2010;Murray

et al., 2021). However, ambient data of direct observation on $\gamma(N_2O_5)$ is still scarce. It is thereby necessary to develop an accurate equipment or method to quantify this parameter on ambient aerosols.

Extensive laboratory experiments have been conducted to derive the values of $\gamma(N_2O_5)$ on aerosols and understand the mechanism of N_2O_5 uptake by various methods, including aerosol flow reactor (Kane et al., 2001;Mozurkewich and Calvert, 1988;Hu and Abbatt, 1997;Thornton and Abbatt, 2005;Thornton et al., 2003;Tang et al., 2014;Bertram and Thornton, 2009a;Cosman et al., 2008;Escoreia et al., 2010;Gaston et al., 2014;Folkers et al., 2003), droplet train reactor (Van Doren et al., 1990;Schweitzer et al., 1998), Knudsen flow reactor (Karagulian et al., 2006) and smog chamber (Wahner et al., 1998;Wu et al., 2020). The $\gamma(N_2O_5)$ was found to be highly variable and dependent on particle chemical composition, acidity, size, phase state and the presence of organic coating using these laboratory methods under controllable conditions (Badger et al., 2006;Bertram et al., 2011;Fried et al., 1994;Griffiths et al., 2009;Gross et al., 2009;Hallquist et al., 2000;McNeill et al., 2006;Mentel et al., 1999;Riemer et al., 2003;Gaston and Thornton, 2016;Escoreia et al., 2010;Gaston et al., 2014;Thornton et al., 2003). While laboratory results have contributed to recognize the mechanism of N_2O_5 uptake and develop $\gamma(N_2O_5)$ parameterizations (Anttila et al., 2006;Bertram and Thornton, 2009b;Davis et al., 2008;Griffiths et al., 2009;Riemer et al., 2009), issues might emerge when quantitatively extended to ambient conditions due to the discrepancy between laboratory conditions and real air mass. For example, much higher reactant and particle concentration usually used in laboratory experiments might induce surface saturation or secondary reactions in a short time period, which lead to the bias of reaction rate used in ambient conditions (Thornton et al., 2003). In addition, the physicochemical properties of ambient aerosol are much more complicated that the model aerosol used in laboratory studies, which led to the laboratory results on model aerosols are difficult to accurately represent what happens on the atmospheric aerosols (Royer et al., 2021;Mitroo et al., 2019).

There have been several methods implemented for field campaigns to indirectly derive $\gamma(N_2O_5)$, simply based on observation of ambient NO_3, N_2O_5, NO_2, O_3, $ClNO_2$, pNO_3^- and

84   other auxiliary parameters without special equipment to capture the decay of N_2O_5 like

85   laboratory ways. These include (1) the linear fit between N_2O_5 (NO_3) lifetime and the product

86   of NO_2 and Sa concentration according to steady state equations (Brown et al., 2002;Brown et

87   al., 2009;Brown et al., 2006;Platt et al., 1984;Wang et al., 2017b;Wang et al., 2017d;Tham et

88   al., 2016;Wang et al., 2017f;Brown et al., 2016), (2) the analysis of production rates of

89   products (pNO_3^- and $ClNO_2$) resulting from N_2O_5 uptake under a stable condition (Mielke et

90   al., 2013;Phillips et al., 2016;Wang et al., 2018b) and (3) box model simulations with an

91   iterative approach to reproduce the evolutions of NO_3-N_2O_5 chemistry within each separate

92   air mass after sunset (McDuffie et al., 2018;Wagner et al., 2013;Wang et al., 2020a;Yun et al.,

93   2018). All these methods contain some specific assumptions and are only applicable in a few

94   special cases.

95   To directly determine the $\gamma(N_2O_5)$ on ambient aerosols, Bertram et al. (2009a) firstly

96   design an entrained aerosol flow reactor to adapt for low atmospheric Sa concentration with

97   easy operation. By switching between filtered and bypass sampling mode, the N_2O_5

98   concentration at the exit of flow tube can be measured in the presence and absence of aerosols,

99   respectively. The pseudo-first-order rate coefficients for N_2O_5 loss on aerosols is thereby

100   derived from the ratio of measured N_2O_5 concentration in these two modes within a duty cycle

101   according to Eq. 1:

$$k_{aerosols} = -\frac{1}{\Delta t}\ln\frac{[N_2O_5]_{\Delta t}^{w/particles}}{[N_2O_5]_{\Delta t}^{wo/particles}} \qquad\qquad \text{Eq. 1}$$

102   where the Δt is the mean residence time of the flow tube, and the $[N_2O_5]_{\Delta t}^{wo/particles}$ and

103   $[N_2O_5]_{\Delta t}^{w/particles}$ are the measured N_2O_5 concentration at the exit of flow tube in filtered and

104   bypass mode, respectively. Assuming the gas-phase diffusion effect is negligible for

105   atmospheric particles and low reaction probability ($\gamma<0.1$) (Fuchs and Sutugin, 1970), $\gamma(N_2O_5)$

106   can then be calculated from Eq. 2:

$$\gamma(N_2O_5) = \frac{4 \times k_{aerosols}}{c \times S_a} \qquad\qquad \text{Eq. 2}$$

107   This method was deployed to measure $\gamma(N_2O_5)$ on ambient particles during two field

108   campaigns (Bertram et al., 2009b;Riedel et al., 2012b) and on aerosols generated in the

109   laboratory (Ahern et al., 2018). While values of $\gamma(N_2O_5)$ were determined to be robust in

110   laboratory experiments, most of data would be dropped under ambient conditions due to the

111   variations of wall loss coefficients (dominated by RH), fresh NO emission, N_2O_5 regeneration

112   and flow pattern inside the flow tube. Based on the above measurement system, Wang et al.

113   (2018c) added NOx, O_3 and Sa measurement on the exit of flow tube and introduce an iterative

114   box model to minimize the potential influences from changing air mass and non-linear

115   response of interference reactions. With the assumption of the equilibrium between NO_3 and

116   N_2O_5, the box model runs backward and forward iteratively to obtain the N_2O_5 loss rate

117   constant in the absence ($k_{het}^{wo/particles}$) and presence ($k_{het}^{w/particles}$) of aerosols respectively.

118   The difference between these two parameters can finally derived the $\gamma(N_2O_5)$ according to Eq.

119   3, assuming the wall loss effect stays consistent.

$$\gamma(N_2O_5) = \frac{4(k_{het}^{w/particles} - k_{het}^{wo/particles})}{c \times S_a} \qquad \text{Eq. 3}$$

120   This iterative approach was demonstrated to be able to buffer against certain fluctuations of

121   air mass and measure $\gamma(N_2O_5)$ in the polluted atmosphere (Yu et al., 2020b).

122   Until now, only few direct measurements of $\gamma(N_2O_5)$ on ambient aerosols have been

123   conducted during field campaigns (Bertram et al., 2009b;Riedel et al., 2012b;Yu et al., 2020a).

124   Even though combining with dataset from indirect approaches (e.g. steady state

125   approximations), it is still challenging to characterize the temporal and spatial distributions of

126     $\gamma(N_2O_5)$ on ambient aerosols. To better investigate the reactive uptake of N_2O_5 on aerosols in

127   different environments, we develop an aerosol flow tube system with newly designed gas

128   circuit and data acquisition procedures to quantify $\gamma(N_2O_5)$ on ambient aerosols. In the

129   following sections, the setup of this system and laboratory characterizations for each part are

130   described in details. Procedures of acquiring and processing data are compared to previous

131   methods and discussed with potential uncertainties. Laboratory tests on model aerosols and

132   field observations are presented to demonstrate its performance under varying ambient

133 conditions.

2 The aerosol flow tube system

135   A schematic of the aerosol flow tube system is shown in Figure 1. The ambient air enters

136 the system from the sampling manifold, mixes with gaseous N_2O_5 source in a Y-tee and flows

137 to aerosol flow tube and detection instruments, as indicated by arrows in the figure. The design

138 of sampling module and aerosol flow tube in this work follows previous work for measuring

139 $\gamma(N_2O_5)$ on ambient aerosols (e.g. Bertram et al., 2009). The major improvement of this system

140 from previous work are continuous monitor of NOx and O_3 concentration before the inlet of

141 flow tube (after sampling air mixing with N_2O_5 source) and the sequential measurements of

142 N_2O_5 concentration both at the inlet and the exit of flow tube within a duty cycle. To achieve

143 the programmed cyclic measurement of these key parameters, we adopted a new design of Y-

144 tee with a static mixer inside and cyclic measurement setup.

145
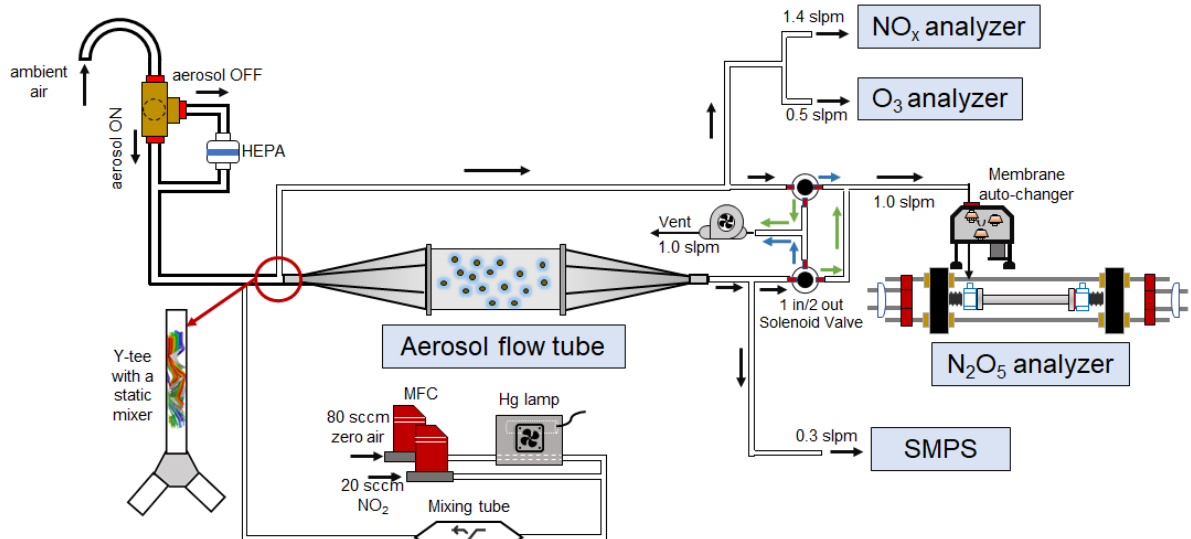
Figure 1. Overall schematic of aerosol flow tube system. The arrows alongside the tube show the flow directions. The black arrows indicate the flow directions consistent during the measurements, green arrows indicate the flow directions active in measuring the exit N_2O_5 and blue arrows indicate the flow directions active in measuring the inlet N_2O_5.

2.1 Sampling manifold

151 The sampling tube is made of a 50 cm long and half inch outside diameter (OD) aluminum

152 tubing, with a curve tip (10 cm radius of curvature) turning the inlet straight down in order to

avoid precipitation. The ambient air is then pass through a three-way stainless-base solenoid ball valve, which is controlled by a time relay to either allow the air to flow directly into a following Y-tee (filter bypass mode) or divert to a HEPA (high efficiency particulate air filter, Whatman) to remove particles (filter inline mode). The HEPA can retain particles at a high efficiency (>99.9%) with low pressure drop and RH difference between filter inline and bypass mode.

2.2 Gaseous N_2O_5 generation

A home-made temperature-controlled gas generator is used to generate gaseous N_2O_5 in-situ via the reaction of O_3 with NO_2 (R1) and the subsequent reaction of produced NO_3 with NO_2 (R2).

$$NO_2 + O_3 \rightarrow NO_3 + O_2 \qquad\qquad\qquad R1$$

$$NO_2 + NO_3 + M \leftrightarrow N_2O_5 + M \qquad\qquad\qquad R2$$

NO_2 is delivered from a compressed gas cylinder (20 ppmv in N_2 diluent gas, Jinghao Corp.). O_3 is generated from the photolysis of O_2 in compressed ultra-pure synthetic zero air at 254 nm, using a commercial mercury lamp (UVP, the USA) fixed inside the generator. The produced O_3 are then mixed with NO_2 in a Teflon chamber for about 2 min under the temperature of 15 ℃, stabilized by a Peltier cooler controlled by proportion integration differentiation algorithm. A PFA tube with polyethylene foam was used to transmit the synthesized N_2O_5 to sampling stream and minimize the influence of ambient temperature variation on N_2O_5 level. The flow rate of NO_2 (20 sccm) and zero air (80 sccm) are controlled by mass flow controller separately at a total of 100 sccm. By changing the flow rate ratio between NO_2 and zero air, the generator can produce N_2O_5 concentration varying from 1 ppbv to 6 ppbv (after dilution in zero air at sampling flow rate of 4.5 slpm). Under the typical measurement condition, an excess of NO_2 concentration is applied to shift the equilibrium towards N_2O_5 production (R2) and suppress the NO_3 concentration to less than 30 pptv, which is expected to decrease the uncertainty of varying NO_3 reactivity (NO, VOCs and heterogeneous loss). The resulted initial N_2O_5 concentration was 4.0 ppbv at the inlet of

178   aerosol flow tube, together with around 50 ppbv of NO_2 and 15 ppbv of O_3. A stability test on

179   N_2O_5 source showed the variation was within 1% for a 24-h continuous operation, with

180   ambient temperature ranging from 0 to 15 °C.

2.3 Aerosol flow tube

182   Air flow enters and exits the flow tube via two identical conical diffuser caps at a diffuser

183   angle of 45°. A 35cm×14 cm inner diameter (ID) cylindrical tube is mounted in the middle

184   of two caps, flanged with screws and nitrile rubber O-rings. All sections of this aerosol flow

185   tube are made of stainless-steel with electro-polished and FEP-coated inside. The exterior of

186   the flow tube is insulated with aluminum coated polyethylene foam 3 cm thick to minimize

187   thermal eddies fluctuation of ambient temperature. The mechanic design of this flow tube

188   follows that used in Bertram et al. (2009), with different length and diffuser angles particularly

189   designed for our typical flow rate. Under the typical flow rate of 2.1 SLPM in the flow tube,

190   the axial velocity in the cylindrical tube section is 0.23 cm·s^{-1} which produces a Reynolds

191   numbers (*Re*) of 22, well below the threshold of laminar flow (*Re*<2100).

192   In front of the flow tube, the synthesized N_2O_5 source is introduced perpendicular to

193   ambient air sampling stream and the mixture then enters a stainless-steel Y-tee for further

194   mixing. The inner surface of Y-tee is electro-polished and coated with SilcoNert 2000 (Silotek

195   Corp.), a technique commonly applied in semiconductor industry, to maintain the transmission

196   efficiency of particles and minimize the loss of N_2O_5 in the meantime. A 10 cm long stainless-

197   steel static mixer is mounted inside the Y-tee in order to swirl the flow and therefore facilitate

198   the mixing between sampling stream and N_2O_5 source in a relatively short distance. The

199   presence of static mixer in front of the inlet also help to improve the flow expansion after

200   entering the flow tube by minimizing recirculation zone, which decreases the wall loss of N_2O_5

201   and particles (Huang et al., 2017). After passing through the static mixer, the mixture of

202   ambient air and N_2O_5 source is split into two flows at the same flow rate, one of which

203   straightly enters the aerosol flow tube and the other one is diverted to measurements of NOx,

204   O_3 and N_2O_5. We measured the concentrations of NOx, O_3, N_2O_5 and Sa at the both exits of

205   Y-tee under typical flow rate for three repeated experiments (Figure 2). Almost the same

206   gaseous concentrations and particle distributions at both exits of Y-tee demonstrate that the

207   N_2O_5 source has been well mixed with the sampling flow.
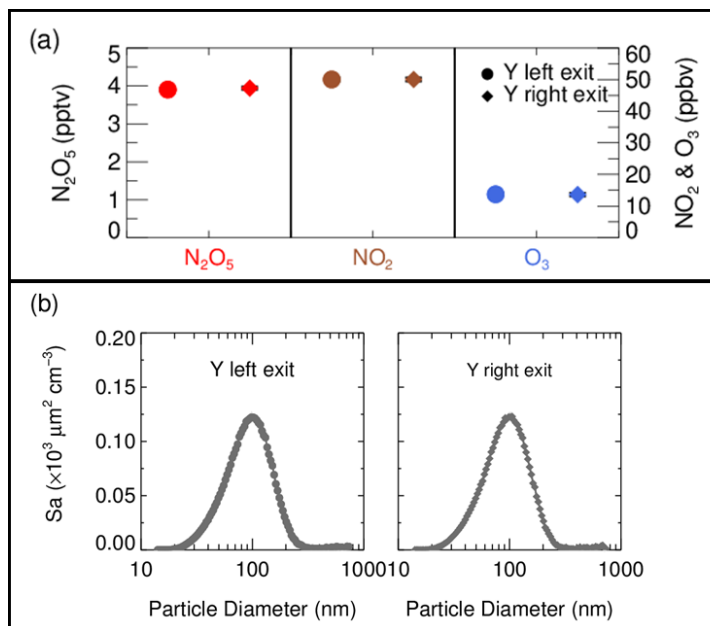
208

209   **Figure 2.** (a) The concentration of N_2O_5, NO_2 and O_3 in the mixture of N_2O_5 source and

210   sampling aerosols measured at each exit of Y-tee; (b) The size distribution of Sa concentration

211   in the mixture of N_2O_5 gas source and sampling aerosols measured at each exit of Y-tee.

2.4 Detection instruments

213   Instruments used in this system are listed in Table 1. A portable cavity-enhanced absorption

214   spectrometer (CEAS) is used to measure N_2O_5 concentration (Wang et al., 2017a) at both inlet

215   and exit of the aerosol flow tube by automatically switching the flow directions (see details in

216   section 2.5). Briefly, the N_2O_5 is thermally decomposed to NO_3 by heating up to 130°C and

217   then quantified according to the extinction coefficient caused by NO_3 absorption in the

218   wavelength window from 640 to 680 nm. A Teflon polytetrafluoroethylene (PTFE) membrane

219   is placed in front of the CEAS to remove particles, which will be replaced with a new one

220   every two hours by a self-designed membrane auto-changer. Laboratory tests have been

221   conducted to quantified the transmission efficiency of N_2O_5 over the membrane (92±3%),

222   sampling tube of CEAS (99.7%) and the inside of CEAS (93.6%). The use of a filter upstream

223   of the CEAS and the procedures of membrane changing have been successfully applied in

224   many field campaigns to measure ambient N_2O_5 (Brown et al., 2016;Kennedy et al.,

225 2011;Wang et al., 2017a;Wang et al., 2017b;Wang et al., 2018a). The loss of N_2O_5 on

226 membrane filter, sampling tube and the detection chamber inside the CEAS were corrected

227 according to transmission efficiency. The detection limit of N_2O_5 was determined to be 2.7

228 pptv (1σ, 60 s) with the measurement uncertainty of 19%. The CEAS has been successfully

229 applied to measure ambient N_2O_5 concentration in several field campaigns and laboratory

230 studies (Chen et al., 2020;Wang et al., 2020a;Wang et al., 2017b;Wang et al., 2020b;Wang et

231 al., 2018b;Wang et al., 2022).

232 **Table 1.** Performance of related instruments incorporated in the flow tube system.

| Parameter	Technique	Time resolution	Detection Limit(1σ)	Accuracy
NO	Chemiluminescence[a]	1 min	200 pptv	±10%
NO_2	Chemiluminescence	1 min	300 pptv	±10%
O_3	UV photometry	1 min	500 pptv	±5%
VOCs	GC-MS/FID[b]	60 min	20-300 pptv	±15%
N_2O_5	CEAS	1 min	2.7 pptv	±19%
Sa	SMPS	5 min	-	±10%
RH&T	Sensor	1 min	-	±0.1%&±0.1K

233 [a] Photolytic conversion to NO through blue light before detection; [b] Gas chromatography

234 equipped with a mass spectrometer and a flame ionization detector;

235 At the inlet of flow tube, NOx concentration is measured via chemiluminescence method

236 equipped with a blue-light photolytic converter (Thermo, Model 42i) and O_3 concentration is

237 also measured via chemiluminescence method by adding excessive NO (Teledyne API, Model

238 T265). Both NOx and O_3 concentration are averaged to 1 min time-resolution. The size

239 distribution of particle number density is measured at the exit of flow tube using a scanning

240 mobility particle sizer (SMPS, TSI 3776), which determines the total Sa concentration

241 covering the range from 13 to 730 nm. Particles larger than this range usually contributed less

242 than 5% of total Sa according to our previous field measurements (Chen et al., 2020) and it is

243 included in the uncertainty analysis (see section 5). A cycle of size scanning is set to around 5

244 min and the derived Sa concentration is then interpolated into 1 min for further calculation.

245 Aerosols pass through a Nafion tubing (MD-700) before entering into SMPS to reduce RH to

246 less than 30%. The dry-state Sa is therefore corrected to wet-state at the RH inside the flow

247   tube for particle hygroscopicity. The growth factor, $f(RH)=1+8.77\times(RH/100)^{9.74}$, used for

248   correction is valid only when RH is within the range from 30 to 90% (Liu et al., 2013). The

249   RH and temperature of flow are continuously measured both before entering and after leaving

250   the flow tube by commercial sensors (Rotronic, Model HC2A-S). The averages of the values

251   obtained at both locations are used to represent the RH and temperature inside the flow tube.

252   In addition, ambient volatile organic compounds (VOCs) are measured in-situ alongside the

253   aerosol flow tube system using an online gas chromatograph mass spectrometer coupled with

254   a flame ionization detector (GCMS-FID) to derive the NO_3 reactivity to VOCs ($k_{NO3\text{-}VOCs}$) in

255   the flow tube.

2.5 Procedures of data acquisition

257   The N_2O_5 concentration is acquired at both inlet and exit of the flow tube within a duty cycle

258   via a CEAS instrument, which is different from that only at the exit of the flow tube in previous

259   studies (Bertram et al., 2009a;Wang et al., 2018c). Each duty cycle consists of once HEPA

260   inline mode for measuring k_{wall} of N_2O_5 and once HEPA bypass mode for retrieving the N_2O_5

261   loss on aerosols. The procedure that measuring N_2O_5 at the inlet of flow tube first and then at

262   the exit is executed within each mode. An exemplary case obtained during a field campaign is

263   shown in Figure 3 to explain this procedure. Within the mode of HEPA inline, N_2O_5 data is

264   firstly acquired at the inlet of the flow tube and then switch to the exit of the flow tube. The

265    $k_{het}^{wo/particles}$, which is the k_{wall} of N_2O_5, can be derived from a box model constrained by these

266   N_2O_5 data (see section 3 for the model description and data processing). The same procedures

267   are executed in the mode of HEPA bypass, except the $\gamma(N_2O_5)$ is derived according to Eq 2.

268   Two three-way valves controlled by a time relay were implemented to realize this procedure

269   in order to avoid the changes of flow condition in the flow tube that could have been caused.

270   As indicated in Figure 1, the blue arrows show the flow directions when measuring the N_2O_5

271   concentration at the inlet of flow tube, while the green arrows shows that for the exit of flow

272   tube. It should be noted that the concentration of NOx and O_3 are always acquired at the inlet

273   of the flow tube and the Sa concentration always at the exit of the flow tube during the

274   operation.
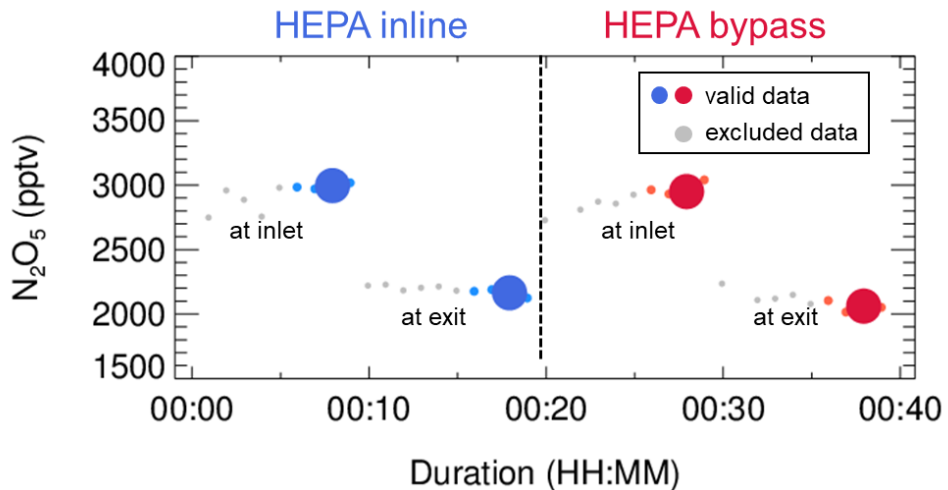
Figure 3. An exemplary case of measured N_2O_5 concentration within a duty cycle. This case was observed on the night of 13 December 2020, with average ambient Sa of 320 μm^2 cm^{-3}. The derived k_{wall} of N_2O_5 and $\gamma(N_2O_5)$ were 0.0023 s^{-1} and 0.035, respectively. The blue dots indicate N_2O_5 concentration measured under the mode of HEPA inline either at the inlet or exit of the flow tube (denoted as texts); the respective averages (blue dots of larger size) are used for deriving k_{wall} (blue square). The red dots indicate N_2O_5 concentration measured under the mode of HEPA bypass either at the inlet or exit of the flow tube; the respective averages (red dots of larger size) are used for deriving the overall rate constant of N_2O_5 loss on the wall and aerosols. The data points in gray are excluded from calculation due to unstable conditions in the flow tube.

In addition, laboratory tests were conducted to determine a suited duration for each duty cycle. During a duty cycle, the duration for each mode should last long enough to develop a stable flow condition for particles or empty particles, while a much longer duration could decrease the measurement time-resolution and leads to large uncertainty due to the fluctuations within a long time period. We measured Sa and N_2O_5 concentration continuously at the exit of flow tube when sampling $(NH_4)_2SO_4$ aerosols. As shown in Figure 4, it took about 15 minutes for particles to rise to a stable level from none or to decrease from a certain level to none, when our system underwent mode switches. The periodical variation of N_2O_5 concentration was consistent with particles. The residence time distribution (RTD) profiles (see in section 4.2) also demonstrated that a pulse injection of NO_2 requires 10~15 minutes to be fully drained out of the flow tube, which to some extent supports the 15-minute time required for complete mixing of N_2O_5. As a result, a typical duration of duty cycle is composed of 40 minutes with

298 20 minutes for each mode, which is similar to that in Bertram et al. (2009). The N_2O_5

299 measurement at the exit of the flow tube in the last 5 minutes of each mode is able to represent

300 valid decays of N_2O_5 under this mode and satisfy the requirements of further data processing.

301
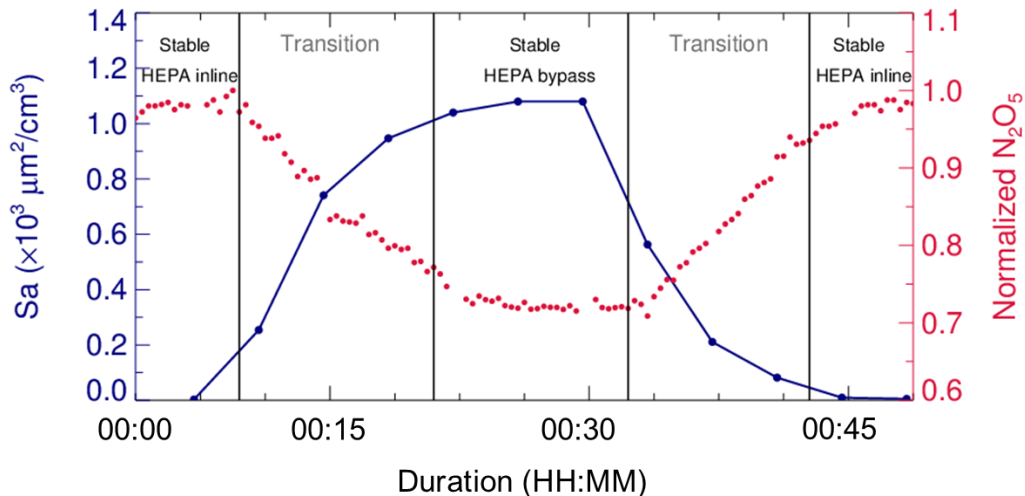
Figure 4. Variations of Sa and N_2O_5 concentration (normalized to peak values) measured at
the exit of flow tube when switching the sampling mode. The phases of species concentrations
in the flow tube approaching stable after a mode switch are denoted as the transition phases.

3 Box model for determination of loss rate coefficients of N_2O_5

3.1 Method description

307 Large uncertainties were found in retrieving $\gamma(N_2O_5)$ on ambient particles according to Eq. 1

308 in a previous flow tube study (Bertram et al., 2009a), due to the dependence of homogeneous

309 reaction rates on sampling modes and the atmospheric variations of parameters related to NO_3-

310 N_2O_5 chemistry (e.g. NO, NO_2, O_3, VOCs, and RH). To minimize these influences, a time-

311 dependent box model constrained by the measurements of N_2O_5 concentration and other

312 auxiliary parameters is applied to calculate loss rate coefficients of N_2O_5 under the mode of

313 HEPA inline and bypass, respectively. The model is able to simulate the reactions related to

314 budgets of NO_3-N_2O_5 chemistry in a dark condition, including R1, R2 and the follows:

$$NO_3 + NO \rightarrow 2\ NO_2 \qquad\qquad R3$$

$$NO_3 + VOCs \rightarrow products \qquad\qquad R4$$

$$N_2O_5 + \text{aerosols or wall} \rightarrow \text{products} \qquad\qquad R5$$

315   The rate constants for reactions R1 to R3 are referenced to IUPAC database. The reaction of

316   VOCs and NO_3 is treated as pseudo-first-order with a rate constant of $k_{NO3-VOCs}$, which is the

317   sum of rate constants for reactions of NO_3 with each VOCs scaled by the concentration of

318   VOCs measured by GC-FID. In this work, there are 30 kinds of measured VOCs having known

319   reaction rate constants with NO_3 included in the model (Table A1). Due to low time-resolution

320   of VOCs measurements (1 h), the $k_{NO3-VOCs}$ is kept constant for each derivation of $\gamma(N_2O_5)$.

321   The suppressed NO_3 concentration is expected to attenuate the influence resulted from the

322   uncertainty of $k_{NO3-VOCs}$ (see discussion in section 5). The reaction R5 represents the loss of

323   N_2O_5 only on the wall in the mode of HEPA inline or on the both wall and particles in the

324   mode of HEPA bypass. The rate constant of R5 is also treated as pseudo-first-order and it is

325   adjustable among different runs.

326   The same procedures of data screening and model operation are applied to both sampling

327   and bypass modes, as shown in Figure 5. For example, in the mode of HEPA inline, the average

328   of NO concentration less than 6 ppbv and the variation of N_2O_5 measured at the inlet of flow

329   tube less than 10% should be validated prior to the following model operation. Under typical

330   concentration of N_2O_5 source we used in this flow tube system, the exit concentration of N_2O_5

331   is detected to be under triple detection limit with initial NO large than 6 ppbv according to our

332   laboratory tests. In ambient condition, high level of NO is usually also accompanied by rapid

333   variation due to fresh emission, which disturbs the decay of N_2O_5 in the flow tube and leads

334   to large uncertainty in deriving its loss rate coefficient. Excluding the cases that N_2O_5

335   measured at the inlet of flow tube varies exceeding 10% can further minimize the uncertainty

336   of N_2O_5 loss rate coefficient resulted from rapid change of NO_3 reactants (NO, VOCs). If the

337   measured data within the duration of a sampling mode satisfies the criteria for data screening

338   described above, the model can therefore simulate the reactions starting from the entrance of

339   flow tube and lasting for 156 s (mean residence time) based on these data. The initial

340   concentrations of $[NO]_{t=0}$, $[NO_2]_{t=0}$, $[O_3]_{t=0}$ and $[N_2O_5]_{t=0}$ are the averages of last-5-min values

341   measured at the inlet of flow tube. The RH and temperature are constrained by the mean values

342   during this sampling mode. By tuning the loss rate coefficient of N_2O_5 (k_{N2O5}) in the way of

343   binary search, we optimized an appropriate k_{N2O5} to ensure that the N_2O_5 concentration output

344   from the simulation is consistent with last-5-min average of N_2O_5 concentration measured at

345   the exit of flow tube within 1 pptv. As a result, this derived k_{N2O5} (aka. $k_{het}^{wo/particles}$) is

346   expected to be the k_{wall} of N_2O_5. The same procedures above are then applied to the data

347   obtained in the mode of HEPA bypass, except that the derived k_{N2O5} (aka. $k_{het}^{w/particles}$)

348   contains the loss rate coefficients of N_2O_5 on the both wall and particles. It should be noted

349   that the above calculation for obtained data is only valid under the variation of RH less than

350   2% within a duty cycle and the k_{wall} of N_2O_5 can then be reasonably assumed to be constant

351   between two successive sampling modes. Therefore, the $\gamma(N_2O_5)$ can be retrieved by the Eq 3,

352   where the last-5-min averages of Sa concentration in the mode of HEPA bypass is used.

353
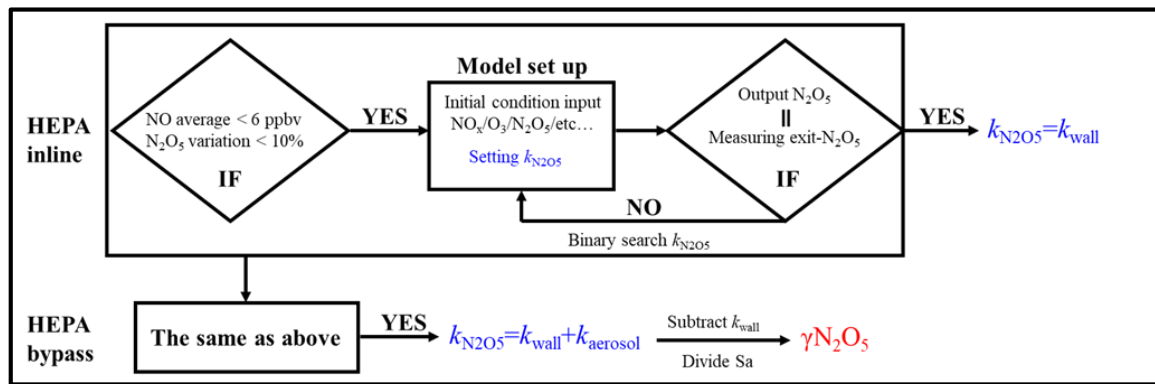
354   **Figure 5**. Flow diagram of $\gamma(N_2O_5)$ derivation through box model method.

3.2 Evaluation of the box model method

356   The box model method is introduced to our flow tube system to overcome the influence from

357   homogeneous reactions and variations of air mass on $\gamma(N_2O_5)$ retrieval. A series of scenarios

358   were provided to evaluate the performance of box model method by both simulations and

359   laboratory experiments. We allow NO, NO_2 and O_3 in the mixture of sampling air at the

360   entrance of the flow tube to vary in a reasonable range, in order to develop the scenarios of

361   different gradients of NO concentration and NO_3 production rates (PNO3). The levels of PNO3

362   was adjusted by NO_2 and O_3 concentrations (O_3 ranging from 10 to 80 ppbv and NO_2 ranging

363   from 50 to 160 ppbv) under the temperature of 283 K and RH of 30%. In simulation studies,

the exit concentration of N_2O_5 would be obtained from the simulated N_2O_5 evolutions with and without particles in the flow tube. To corroborate the results estimated by simulations, laboratory tests were performed on $(NH_4)_2SO_4$ aerosols to measure the exit concentration of N_2O_5 under varying NO concentration. The $\gamma(N_2O_5)$ on particles are then calculated according to Eq 1&2 or by box model method described above.

As shown in Figure 6(a), the exit concentration method ($\gamma(N_2O_5)$ exit-conc., derived directly by Eqs. 1-2) underestimates $\gamma(N_2O_5)$ and the extent of underestimation increases with PNO_3 levels in simulation tests. Similarly, the exit concentration method underestimates $\gamma(N_2O_5)$ by 50 to 60% with PNO_3 of 1.0 ppbv h^{-1} in the laboratory tests (Figure 6(b)). Noted that the $\gamma(N_2O_5)$ was determined to be at around 0.01 by box model method over the NO range from 0 to 6 ppbv, which agrees well with previous laboratory observation of $\gamma(N_2O_5)$ on $(NH_4)_2SO_4$ aerosols within uncertainty (Badger et al., 2006;Hallquist et al., 2003;Kane et al., 2001). The cause of $\gamma(N_2O_5)$ exit-conc. underestimation is mainly due to the in situ N_2O_5 production in the flow tube. With a continuous production of NO_3 via the reaction of NO_2 and O_3 and rapid heterogeneous loss of N_2O_5 in the flow tube, the equilibrium between NO_3 and N_2O_5 always shifts to the production of N_2O_5, and masking the actual amount of N_2O_5 removal. In the mode of HEPA bypass, the N_2O_5 consumes faster than the other mode due to the addition of particles, which further facilitates the N_2O_5 formation through the equilibrium. Previous studies also found similar impacts from N_2O_5 production on retrieving $\gamma(N_2O_5)$ in the aerosol flow tube (Bertram et al., 2009a;Wang et al., 2018c). However, the discrepancy of $\gamma(N_2O_5)$ derived by two methods is much less dependent on the NO concentration, at least within the prescribed range, due to relatively small ratio of NO_3/N_2O_5 in the N_2O_5 source. The absence of dependence between NO concentration and $\gamma(N_2O_5)$ also indicates that this aerosol flow tube system can buffer against NO within the range from 0 to 6 ppbv under typical operating condition. However, this is not always the case when there is a rapid fluctuation of NO in a real atmosphere, which might lead to intractable uncertainty and is therefore excluded from further analysis according to the criteria of data screening.
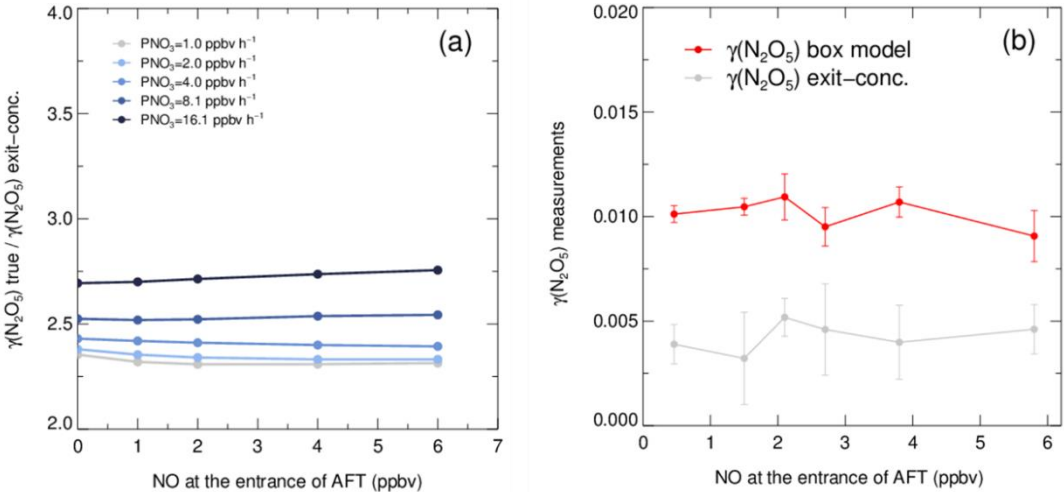
Figure 6. Simulated and laboratory tests on performance of box model method and exit concentration method for $\gamma(N_2O_5)$ derivation. (a) The ratios of given $\gamma(N_2O_5)$ ($\gamma(N_2O_5)$ true) over exit concentration derived $\gamma(N_2O_5)$ ($\gamma(N_2O_5)$ exit-conc.) determined from simulated scenarios. The $\gamma(N_2O_5)$ derived by box model method is exactly the same as $\gamma(N_2O_5)$ true. The ratios vary with NO concentration and the lines are color coded by PNO_3 values. Both NO concentration and PNO_3 represent the values at the entrance of aerosol flow tube. (b) $\gamma(N_2O_5)$ measurements on lab-generated $(NH_4)_2SO_4$ aerosols under different gradients of NO with constant RH of 50% and PNO_3 typically generated from our N_2O_5 source. The red line shows the $\gamma(N_2O_5)$ derived by box model method and gray line shows the $\gamma(N_2O_5)$ derived by exit concentration method. The NO concentrations are measured at the entrance of aerosol flow tube.

In comparison to the work by Bertram et al. (2009) and Wang et al. (2018), the combination of above box model method and the improved flow tube system in this study has progress in the following aspects. First, the dynamic quantification of k_{wall} of N_2O_5 within each duty cycle based on the constraint of sequentially measured N_2O_5 source is helpful to provide accurate data for both k_{wall} and $\gamma(N_2O_5)$ retrieval. The k_{wall} in ambient conditions could deviate from the results from laboratory tests (Figure B1) due to temperature variation and particles adsorption, which leads to large uncertainty when calculating $\gamma(N_2O_5)$ without the frequent determination of k_{wall}. While the k_{wall} was also determined frequently in the flow tube of Wang et al. (2018), the N_2O_5 source they used for k_{wall} and $\gamma(N_2O_5)$ retrieval is an assumed stable value instead of an observed one. Second, the concentrations of initial NO, NO_2, O_3 and N_2O_5 at the entrance of the flow tube, and exit N_2O_5 are obtained through programed cyclic

414 measurements in this work, which can reduce the uncertainties by adding the model constraints.

415 It is different from the iterative box model used in Wang et al. (2018) as we enable a

416 straightforward simulation of NO_3-N_2O_5 chemistry occurring in the flow tube, instead of

417 estimating the initial NO_2 and O_3 with assumed NO profile and stable N_2O_5 source based on

418 backward simulations. In ambient conditions, the initial N_2O_5 concentration can be largely

419 influenced by air mass conditions (especially NO concentration and temperature). Figure B2(a)

420 presents box whisker plot of N_2O_5 and NO concentration at the flow tube entrance during a

421 field campaign, which shows a much larger variation of N_2O_5 than in lab condition (<1%). As

422 a result, the box model would underestimate $\gamma(N_2O_5)$ by using a fixed initial N_2O_5

423 concentration under certain circumstances (Figure B2(b)). Third, we simulate NO_3-N_2O_5

424 relationship via specific reactions rather than approximating it in equilibrium and introducing

425 the equilibrium coefficient (Keq) into calculation. Calculating NO_3 or N_2O_5 concentration by

426 Keq could induce large bias (up to 90%) under the high aerosol loading and low temperature

427 (Chen et al., 2021).

4 Laboratory characterizations

4.1 Particle transmission efficiency

430 The transmission efficiency of particles in the sampling module and flow tube are estimated

431 respectively in Figure 7. In the laboratory, pure ammonia nitrate (($NH_4)_2SO_4$) aerosols were

432 generated from an atomizer loading with 0.1 M ($NH_4)_2SO_4$ solution. The RH and concentration

433 of produced aerosols flow was conditioned in a glass bottle (~2 L) by introducing a humidified

434 dilution flow of ultrahigh-purity N_2. As a result, aerosols in different concentrations

435 (1000~4500 μm^2 cm^{-3}) and under a range of RH (20~70%) were applied to test the

436 transmission efficiency. Figure 7(a) shows the loss of total Sa concentration in the sampling

437 module and flow tube are 8±1% and 10±2% on average, respectively. We found that the

438 fraction of particles loss is mainly caused by particles smaller than 100 nm. This is most likely

439 due to the turbulence generated by static mixer and the recirculation in the flow tube. Large

440 particles are prone to stay within the main flow direction, whereas small particles readily

441 adsorb on the walls by the entrainment of turbulence or recirculation. In addition, the particles

442 distribution measured at the exit of flow tube with HEPA inline (gray line in Figure 7(a))

443 demonstrated its capability of removing almost all particles (>99.5%) at the typical flow rate.

444 The same transmission efficiency was also found on ambient aerosols (Figure 7(b)) as that on

445 laboratory-generated aerosols. The results we obtained from above particle transmission

446 experiments are similar to the findings of Bertram et al. (2009).
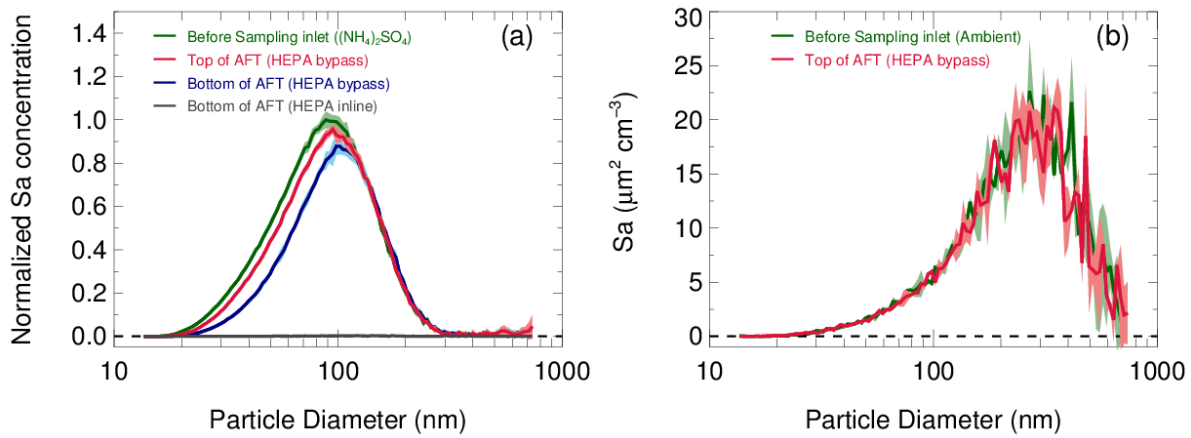
447

448 **Figure 7**. (a) Particles transmission determined by sampling laboratory-generated $(NH_4)_2SO_4$

449 aerosols. Aerosols at different concentrations and RH levels are used in experiments and the

450 size distribution of Sa concentration are normalized to the peak values. The normalized size

451 distribution of Sa concentration measured before sampling inlet (green line), at the inlet of

452 flow tube with HEPA bypass (red line) and at the bottom of flow tube with HEPA bypass

453 (blue line) are shown respectively. Under the mode of HEPA inline, the Sa concentration was

454 almost zero at the bottom of flow tube (gray line). The shadows indicate the standard

455 deviations of the normalized Sa concentration for all experiments. (b) Particles transmission

456 determined by sampling ambient particles.

457 4.2 Residence time in the flow tube

458 The method of residence time distribution (RTD) was applied to estimate the average reaction

459 time of the gas species in the flow tube (residence time). In comparison to ideal plug flow, the

460 RTD method can better describe actual behavior of the flow in practice and determine the

461 mean residence time more accurately (Danckwerts, 1953). Several studies have also used this

462 RTD method to determine the residence time in the flow tube (Huang et al., 2017; Wang et al.,

463 2018c; Lambe et al., 2011).

464   The RTD profiles were obtained by introducing a 2 s pulse of NO_2 gas diluted in N_2 into

465   the flow tube under RH less than 1%. NO_2 is relatively inert against the flow tube wall coated

466   with FEP and was measured at the exit of the flow tube by a CEAS (Li et al., 2021) at high

467   time-resolution (2 Hz). A three-way solenoid valve combined with a time relay was

468   implemented to control the pulse in order to avoid the disturbance on flow condition from the

469   injection. Experiments were performed under typical operation. The mean residence time (t_{ave})

470   can be derived from the each RTD profile according to Eq. 4,

$$t_{ave} = \frac{\sum_{i=0} C_i \times t_i}{\sum_{i=0} C_i},$$
Eq. 4

471   where the C_i is the concentration of NO_2 recorded at the time step t_i. From the RTD profiles

472   of NO_2 injection experiments in Figure 8, the determined t_{ave} was 156±3 s. This value is 19%

473   less than the space time (τ_{space}, flow tube volume divided by operation flow rate, 192.6 s). It

474   has also been found that the assumption of ideal plug flow overestimated the residence time

475   in previous flow tube experiments (Lambe et al., 2011;Huang et al., 2017;Wang et al., 2018c),

476   which could lead to underestimation of the derived k_{N2O5}. The residence time of current set up

477   is designed for investigating $\gamma(N_2O_5)$ in typical episode days with medium to high aerosol

478   loadings (the Sa concentration usually larger than 500 um^2 cm^{-3}) in polluted regions. As shown

479   in Section 5, the detection limit of this system is 6.4×10^{-4} with Sa of 500 um^2 cm^{-3}, which is

480   well below the most of previous ambient $\gamma(N_2O_5)$ results ranging from 1×10^{-3} to >0.1 in

481   polluted regions of China (Wang et al., 2020a;Wang et al., 2017d;Wang et al., 2017e;Xia et al.,

482   2019). The residence time determined in this work is also slightly higher than 149 s that

483   reported in a previous work focusing on investigating $\gamma(N_2O_5)$ in polluted regions(Wang et al.,

484   2018c). In addition, the residence time for this flow tube can be extended to over 300 s to

485   satisfy the $\gamma(N_2O_5)$ measurement requirements under low Sa by reducing the flow rate of air

486   passing through, which is controlled by an extra pump.

487
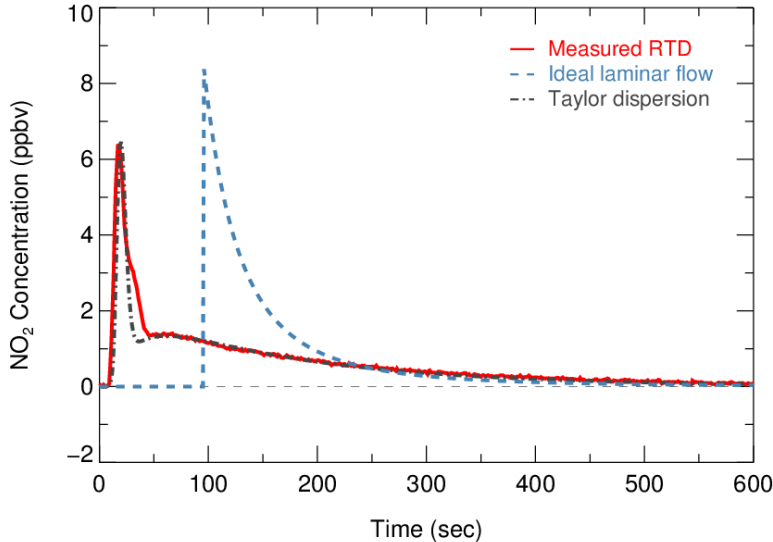
Figure 8. Residence time distribution derived by sampling NO_2 gas. Red solid line indicates the measured RTD profiles. The calculated RTD of ideal laminar flow (without dispersions) and the Taylor dispersion model fitted to measurements are shown as blue dash line and dot-dash line, respectively.

Two theoretical RTDs were calculated, namely ideal laminar flow and Taylor diffusion, besides the measured RTD, intending to reflect the fluid field inside the flow tube. The ideal laminar flow describes the flow without dispersion. The velocity profile of ideal laminar flow is parabolic, with the fluid in the center of the tube moving the fastest. According to the following Eq. 5, the RTD of ideal laminar flow is scaled by the integrated concentration of NO_2 and presented as the blue dash line in Figure 8.

$$\begin{cases} 0, & t < 0.5\tau_{space} \\ \dfrac{\tau_{space}^2}{2t^3}, & t \geq 0.5\tau_{space} \end{cases}, \qquad \text{Eq. 5}$$

While the determined Re is well within the laminar flow threshold, the measured RTD occurs earlier than theoretical laminar flow condition and exhibits a broaden distribution. The discrepancy between them indicates that the dispersions or potential secondary flows could dominate the flow regime. Instead, an improved Taylor dispersion model (shown as the gray dot-dash line in Figure 8) is able to reproduce the measured RTD, which was previously implemented in the characterization of photooxidation flow reactors (Lambe et al., 2011). Two flow patterns with distinct effective diffusivities (0.02 and 0.51 derived from best fit) were considered in this dispersion model. An implication from the characteristics of the model is

21

506 that two flow components consist of the flow regime: a direct flow path through the flow tube

507 with less diffusion and a secondary flow path representing the recirculation in the dead zone

508 that induced by temperature gradient and significant diffusions (Huang et al., 2017).

4.3 N_2O_5 wall loss

510 Laboratory tests were conducted to quantify the k_{wall} of N_2O_5 under different levels of RH with

511 HEPA inline. As shown in Figure 9, the k_{wall} of N_2O_5 gradually increase from 0.002 s^{-1} in a dry

512 condition to 0.006 s^{-1} when RH is 70%. The level of k_{wall} is less than the result of Wang et al.

513 (2018c) but higher than Bertram et al. (2009a) as indicated in Table 2. In addition, the flow

514 tube was rinsed with deionized water every week during the field campaigns to remove the

515 build-up of particles, which might increase the hygroscopicity of the internal surface and thus

516 the k_{wall} of N_2O_5 in a wet condition. Uncertainty in $\gamma(N_2O_5)$ derivation resulted from the

517 variation of k_{wall} related to RH is discussed in section 5.
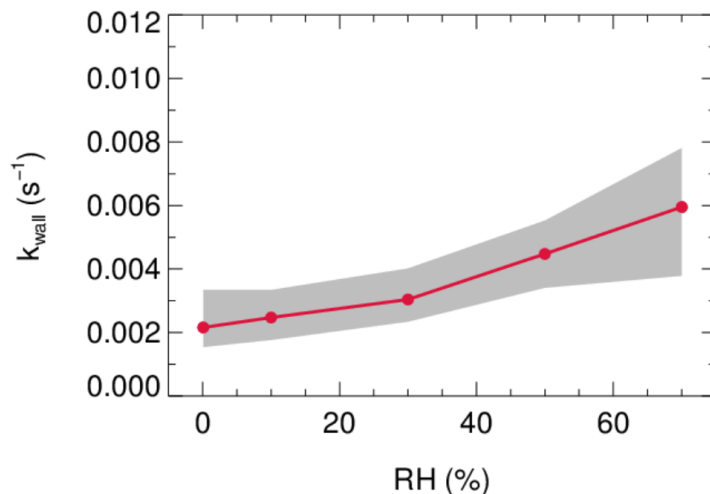
518

519 **Figure 9**. The dependence of pseudo-first-order wall loss coefficient (k_{wall}) of N_2O_5 in the

520 FEP-coated aerosol flow tube.

521 **Table 2**. Summary of the k_{wall} of N_2O_5 for the existing aerosol flow tube deployed in field

522 campaigns.

RH range	k_{wall} range ($\times 10^{-3}$ s^{-1})	References
5~50%	0.5~3	Bertram et al., 2009
20~70%	4~9	Wang et al., 2018
0~70%	2~6	This work

4.4 Demonstration of $\gamma(N_2O_5)$ measurements on model particles

$\gamma(N_2O_5)$ measurements by current aerosol flow tube system equipped with box model method were performed on lab-generated $(NH_4)_2SO_4$ aerosols over a range of RH. The system was operated at room temperature of 295K with N_2O_5 concentration of 4.0 ppbv at the entrance of flow tube. We conditioned the RH of generated aerosols by introducing dry N_2 gas dilution, which could decrease the RH level down to 10~55%, starting from over 95% where $(NH_4)_2SO_4$ aerosols are expected to be in aqueous state. The resulting Sa concentrations of aerosols were around 600 $\mu m^2 \cdot cm^{-3}$. As shown in Figure 10, the observed $\gamma(N_2O_5)$ values were below 0.01 when RH was within 40% and significantly rose up to 0.02 with higher RH. The dependence of $\gamma(N_2O_5)$ on RH and the exact values are well consistent with previous laboratory results on $(NH_4)_2SO_4$ aerosols (Badger et al., 2006;Hallquist et al., 2003;Hu and Abbatt, 1997;Kane et al., 2001;Mozurkewich and Calvert, 1988), which shows that the setup of our instrument has good practicability. A large standard deviation of $\gamma(N_2O_5)$ found at RH of 39% is possibly due to the unstable phase transition of $(NH_4)_2SO_4$ particles, as its efflorescence RH is reportedly from 35 to 48% (Martin, 2000).
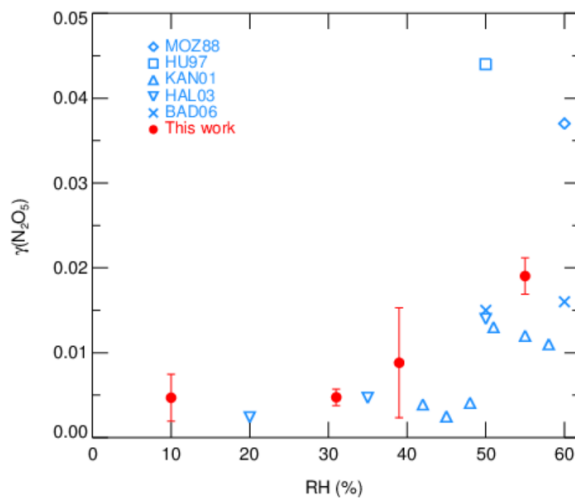
Figure 10. The dependence of $\gamma(N_2O_5)$ on RH for laboratory-generated $(NH_4)_2SO_4$ aerosols. The red points with standard deviations represent the values measured by current aerosol flow tube system in this work. Previously reported values are indicated in blue marks.

5 Uncertainty analysis and detection limit

The uncertainty of $\gamma(N_2O_5)$ is in relevance to the measurement uncertainties of each instrument and rapid fluctuations of various parameters. As outlined before, the 5-min averages of N_2O_5 concentration measured at the inlet and exit of the flow tube were used for calculating $\gamma(N_2O_5)$ via the box model method. The potential variations within these selected time periods would therefore lead to relative errors. For example, the variations of N_2O_5 concentration is resulted majorly from the rapid changes of ambient NO and less from variations of VOCs, NO_2, O_3 as well as N_2O_5 gas source itself (1% in 24 hours). A cutoff of 10% for N_2O_5 variation was implemented to filter out the air mass that was too unstable for valid analysis, according to our prescribed criteria of data screening. It consequently leads to 10% uncertainty in the average of N_2O_5 and can translate into a deviation of 2% in $\gamma(N_2O_5)$ with the $\gamma(N_2O_5)$ at 0.02, Sa at 800 $\mu m^2 \cdot cm^{-3}$ and other parameters (shown in Table 3) representing the typical inlet values measured during the field campaign (described in section 6). Similarly, cases that over 2% variation in RH exists between the HEPA inline and bypass mode are excluded from analysis, owing to its significant influence on k_{wall} of N_2O_5 in the flow tube. By assuming a consistent k_{wall} in successive sampling modes, the potential variations in RH could lead to uncertainty in $\gamma(N_2O_5)$ from $\pm 8 \times 10^{-4}$ at RH of 20% to $\pm 2 \times 10^{-3}$ at RH of 70%, respectively, with the Sa at 800 μm^2 cm^{-3}. In addition, the $k_{NO3-VOCs}$ is treated as constant in a duty cycle due to the limit of time resolution of VOCs measurements. A variation of ± 0.01 s^{-1} in $k_{NO3-VOCs}$ only induces less than $\pm 1\%$ uncertainty in $\gamma(N_2O_5)$ for more than 95% cases obtained during the field campaign. All the impacts from inherent instruments uncertainties and variations of different parameters are thereby considered in Monte Carlo simulations to assess the overall uncertainty of $\gamma(N_2O_5)$. The basic simulation is initialized with the typical conditions measured at the inlet of the flow tube during the field campaign and repeatedly performs the procedures of determining $\gamma(N_2O_5)$ via the box model method 1000 times. In each run, all parameters were allowed to vary independently within a prescribed range. The basic simulation condition and variation range are presented in Table 3.

**Table 3.** Parameters involved in the Monte Carlo simulations.

Parameters	Value [a]	Variation range [b]
NO	1 ppbv	±10%
NO_2	70 ppbv	±10%
O_3	10 ppbv	±5%
Inlet N_2O_5	4 ppbv	±19%
Exit N_2O_5 [c]	2.2 ppbv	±19%
Temperature	273 K	±0.1 K
RH [d]	30 %	±1%
$k_{NO3-VOCs}$	0.01 s^{-1}	±0.01 s^{-1}

570   [a] Values used for initializing Monte Carlo simulations in a basic scenario; [b] Ranges within

571   which each parameter can vary independently; [c] Determined from the case that $\gamma(N_2O_5)$ is at

572   0.02, Sa is at 800 $\mu m^2 \cdot cm^{-3}$ and other parameters are shown in this table; [d] The RH and its

573   variation can be transformed into values in k_{wall} of N_2O_5 via the fitting function derived from

574   Figure 9.

575   The resulting $\gamma(N_2O_5)$ values from Monte Carlo simulations under the basic scenario are

576   shown as frequency distributions in Figure 11(a). This distribution can be fitted by a Gaussian

577   function and the standard deviation (1σ) of Gaussian distribution is regarded as the overall

578   uncertainty of $\gamma(N_2O_5)$, which is $\pm 9 \times 10^{-4}$ (4.5% relative to true $\gamma(N_2O_5)$). The uncertainty of

579   Sa measurements and unmeasured particles larger than 730 nm (usually less than 5% of total

580   Sa) would together introduce an extra 16% uncertainty to $\gamma(N_2O_5)$.

581   We further found that the uncertainty of $\gamma(N_2O_5)$ could be sensitive to the measurement

582   conditions. With higher O_3, potential variations of NO and $k_{NO3-VOCs}$ will induce larger

583   uncertainty of $\gamma(N_2O_5)$ (Figure 11(b)), as it enhances the abundance of NO_3 and N_2O_5. In

584   comparison, the low O_3 in the basic scenario suppressed the side formation of NO_3 in the flow

585   tube, limiting the aggravation of $\gamma(N_2O_5)$ uncertainty from the increase of NO and NO_2. The

586    $\gamma(N_2O_5)$ uncertainty is also positive correlated with RH and T. As is discussed before, the k_{wall}

587   of N_2O_5 increases with RH level, which can amplify the potential bias of k_{wall} at a higher RH

588   level. The equilibrium between NO_3 and N_2O_5 shifts towards the decomposition of N_2O_5 at

589   higher T, leading to larger uncertainty of $\gamma(N_2O_5)$ caused by potential variations of NO and

590 $k_{NO3-VOCs}$. The overall uncertainty of $\gamma(N_2O_5)$ therefore rises to 8.2% at the RH of 70% and to

591 14.4% at the temperature of 293K (Figure 11(c)), with NO, NO$_2$, O$_3$, $\gamma(N_2O_5)$ and Sa keeping

592 the same as the basic scenario. In addition, Monte Carlo simulations were also performed for

593 different $\gamma(N_2O_5)$ values ranging from 0.01 to 0.08. The uncertainty of $\gamma(N_2O_5)$ clearly

594 decreased with the $\gamma(N_2O_5)$ (Figure 11(d)). A lower $\gamma(N_2O_5)$ weaken the impacts N$_2$O$_5$ uptakes

595 has on the budgets of NO$_3$ and N$_2$O$_5$, which causes the $\gamma(N_2O_5)$ derivation to be more

596 susceptible to uncertainties of other parameters and then increases the uncertainty of $\gamma(N_2O_5)$.
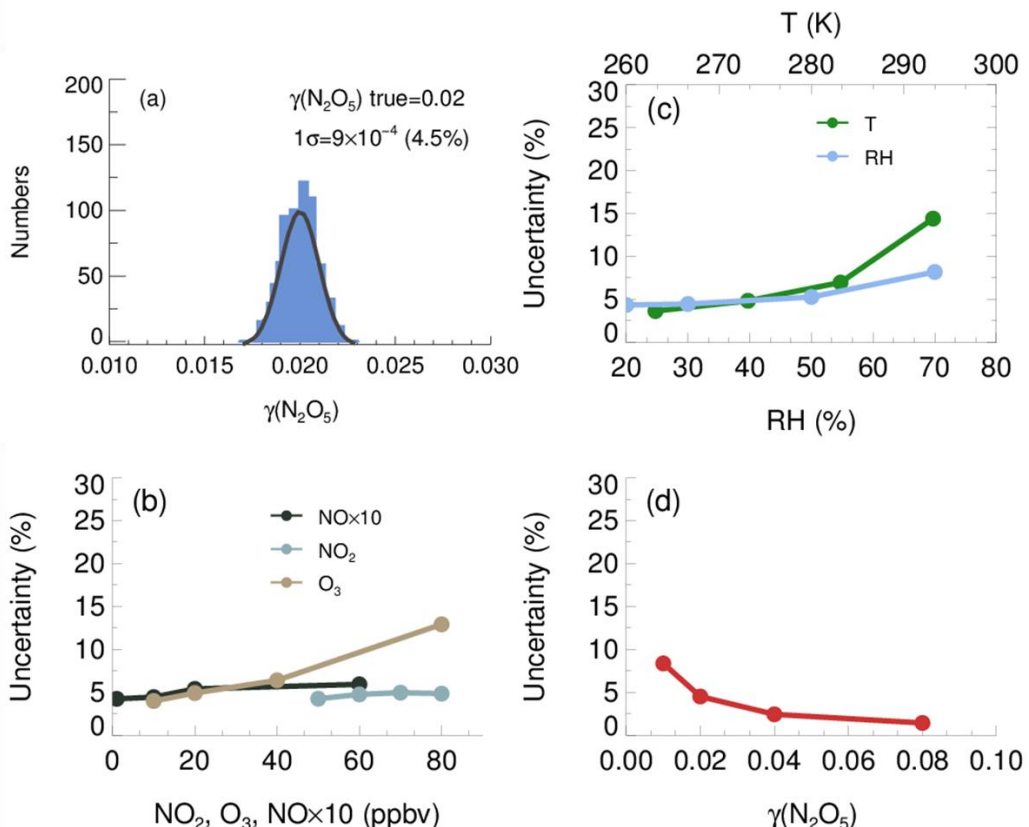
597

598 **Figure 11**. The uncertainty of $\gamma(N_2O_5)$ determined from the Monte Carlo simulations. (a)

599 Histogram distribution of $\gamma(N_2O_5)$ generated from a Monte Carlo simulation (1000 single runs)

600 in the basic scenario (shown as Table 3), where the overall uncertainty of $\gamma(N_2O_5)$ was

601 determined to be $\pm 9 \times 10^{-4}$; (b) dependence of the uncertainty of $\gamma(N_2O_5)$ on NO, NO$_2$ as well

602 as O$_3$; (c) dependence of the uncertainty of $\gamma(N_2O_5)$ on RH and T; (d) dependence of the

603 $\gamma(N_2O_5)$ uncertainty on $\gamma(N_2O_5)$ level.

604   In addition, the mean residence time used in the box model method could bias the retrieved

605 $\gamma(N_2O_5)$ due to the non-normal distribution of residence time with a discernable tail. The

606 reactants entrained by those slower streamlines close to the wall will take much longer time to

26

607   reach the exit of the flow tube than that by the centerline. In order to evaluate the uncertainty

608   caused by the distribution of residence time, we first performed simulations of N_2O_5 decay in

609   the flow tube under the basic scenarios and calculate the exit N_2O_5 concentration according to

610   the probability distribution function derived from RTD profile. Then the $\gamma(N_2O_5)$ can be

611   retrieved from the box model method running for the duration of mean residence time,

612   constrained by this calculated exit N_2O_5 concentration. The result shows that the use of mean

613   residence time produces 32% underestimation of $\gamma(N_2O_5)$ in the basic scenario. The extent of

614   underestimation is most sensitive to the level of $\gamma(N_2O_5)$ and RH. In short, when taking all the

615   factors and their corresponding varying ranges discussed above into consideration, the overall

616   uncertainty of $\gamma(N_2O_5)$ determined from Monte Carlo simulations is in the range of 16-43%.

617   To directly compare with previous studies, at 0.03 $\gamma(N_2O_5)$ with 1000 μm^2 cm^{-3} Sa, the

618   uncertainty is calculated to be 19% which is lower than that ~24% in Bertram et al (2009) and

619   that ranging 37%~40% in Wang et al (2018).

620   In order to determine the detection limit of the current aerosol tube system, the continuous

621   blank measurements in zero air were performed with settled operation procedures. Within per

622   duty cycle (40 minutes), one k_{wall} of N_2O_5 and one $\gamma(N_2O_5)$ can be derived in pair. In total, we

623   obtained 56 sets of result. The detection limit of k_{N2O5} on aerosols is 2.1×10^{-5} s^{-1}, derived from

624   1σ of the Gaussian function fitted to this distribution. It is equivalent to 0.0016 for the detection

625   limit of $\gamma(N_2O_5)$ with a low Sa condition of 200 μm^2 cm^{-3} (Figure 12(a)), and 0.00064 for the

626   detection limit of $\gamma(N_2O_5)$ with a moderate Sa condition of 500 μm^2 cm^{-3} (Figure 12(b)). This

627   result indicates that the flow tube system has capability of quantifying $\gamma(N_2O_5)$ for most cases

628   even under a low aerosol-loading environment.
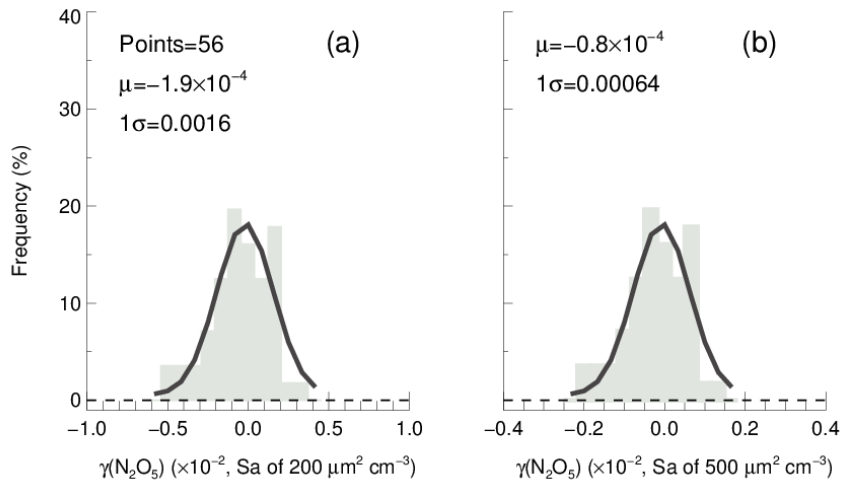
Figure 12. The $\gamma(N_2O_5)$ derived from blank measurements in histogram distribution plot. The $\gamma(N_2O_5)$ was calculated from k_{N2O5} by Eq 2 with Sa of (a) 200 μm² cm⁻³ and (b) 500 μm² cm⁻³, respectively, under the temperature of 293K. The Gaussian function is fitted to the distribution and plotted in black line. The 1σ from Gaussian fit is regarded as the detection limit.

6 Performance in the field campaign

The aerosol flow tube system was successfully deployed to measure $\gamma(N_2O_5)$ on ambient aerosols in Beijing lasting for 20 days during the December of 2020. The sampling site was at the campus of Peking University, which is located in the city center of Beijing surrounded by major roads with heavy traffic. Therefore, this site represents an area with large amount of fresh emission of NOx and other anthropogenic sources. The system was mounted in the top floor of a building, about 15 m height above the ground. The sampling manifold was placed in open air and the ambient aerosols could directly enter the inlet of the manifold without additional sampling tubes. During the period of measurement, the averages of ambient temperature, RH, NO, NO_2, O_3 and Sa were 273 ± 3 K, 25 ± 12 %, 23 ± 36 ppbv, 23 ± 12 ppbv, 16 ± 15 ppbv and 409 ± 249 μm² cm⁻³, respectively. The NO and Sa levels could vary by 2 orders of magnitude due to the periodical switch between clean air mass from the north and pollutants accumulated by local emission.

A total of 99 valid $\gamma(N_2O_5)$ values were determined from the measurements based on the criteria of data screening described in section 3.1. We found that $\gamma(N_2O_5)$ was 0.042 ± 0.026 on average with a median of 0.035, ranging from 0.0045 to 0.12 (Figure 13). These results are

28

650   comparable to that previously determined in the North of China using various different

651   methods (Wang et al., 2017b;Wang et al., 2018b;Wang et al., 2017d;Wang et al., 2017e;Xia et

652   al., 2019;Yu et al., 2020a). The k_{wall} of N_2O_5 corresponding to valid $\gamma(N_2O_5)$ measurements

653   was rather stable at an average of 0.0021±0.0007 s^{-1}, which was consistent with the values

654   determined at similar RH levels in the laboratory tests. It somehow reflected the robustness of

655   the status of the flow tube system and the derived results.

656   In the current system, the N_2O_5 concentrations measured at both entrance and exit of the

657   flow tube are sensitive to the NO fluctuations within the timescale of one sampling mode,

658   which can induce large uncertainty on calculating $\gamma(N_2O_5)$. With our stringent criteria of data

659   screening, the cases of drastic NO fluctuations were excluded from the analysis. Hence, the

660   majority of valid $\gamma(N_2O_5)$ for this campaign were obtained during the periods of the NO below

661   2 ppbv, when the clean air mass was dominant at this urban site. Meanwhile, the Sa

662   concentration within clean episodes were also lower than other periods, with an average of

663   159 μm^2 cm^{-3}. The derived k_{N2O5} ranged from 2.1×10^{-5} to 1.6×10^{-3} s^{-1} well above the

664   detection limit, which demonstrated the robustness of results even subject to low ambient Sa

665   conditions. In order to improve the applicability of $\gamma(N_2O_5)$ measurements, future

666   development is suggested to prioritize the reduction or removal of NO level (at least the

667   fluctuation of NO) in the sampling system before the entrance of flow tube without the cost of

668   particles transmission efficiency.
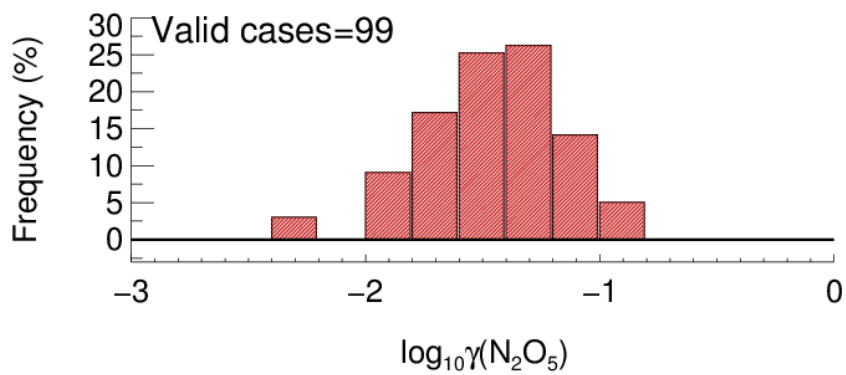
669

670   **Figure 13**. The histogram distribution of measured $\gamma(N_2O_5)$ for valid cases.

7 Summary and conclusion

We report a new development of an aerosol flow tube system coupled with detailed box model to derive $\gamma(N_2O_5)$ directly on ambient aerosols. The unique feature of this system is that the sequential N_2O_5 measurement at the both ends of flow tube was applied to improve the accuracy in quantifying $\gamma(N_2O_5)$, by taking it as a constraint for the box model to reproduce the decay of introduced N_2O_5 gas source in the flow tube. With the consideration of detailed chemistry related to N_2O_5, the proposed approach was testified to refrain from the interference of side reactions, induced by the additional N_2O_5 generation, NO titration in the flow tube and variations of air masses between successive sampling modes.

A series of laboratory tests were performed to characterize factors affecting $\gamma(N_2O_5)$ derivation and demonstrate its applicability on $(NH_4)_2SO_4$ aerosols. The uncertainties associated with instruments used in the system and potential fluctuations of various parameters were thoroughly discussed in the uncertainty analysis, and we estimated the overall uncertainty of $\gamma(N_2O_5)$ to be 16-43% which is subject to NO, NO_2, O_3, meteorological parameters, residence time and $\gamma(N_2O_5)$ value itself. The detection limit of $\gamma(N_2O_5)$ was quantified to be 0.0016 at the aerosol surface concentration (Sa) of 200 μm^2 cm^{-3}. We deployed this system for field observations of $\gamma(N_2O_5)$ at an urban site in Beijing, where strong anthropogenic emission and frequent switch of air mass were encountered. The obtained $\gamma(N_2O_5)$ was in comparable level to previously reported values in northern China and demonstrated the robustness of this system during low NO episodes. Further investigations on N_2O_5 heterogeneous chemistry for both laboratory-generated and ambient particles are also available by the introduced approach.

Appendix A: Measured VOCs used to calculate NO$_3$ reactivity in the box model method

A total of 59 kinds of VOCs were measured by GC-FID-MS in this work, half of which had known rate constants that can be used to parameterize the reaction of NO$_3$ with VOCs (mainly compose of alkenes and aromatics) in γ(N$_2$O$_5$) retrieval by box model method (see also section 3). Their rate constants were obtained from MCM331 or IUPAC and the values at 298K are listed in Table A1.

**Table A1.** VOCs used to calculate NO$_3$ reactivity (k_{NO3}) in the box model method

| Species	k_{NO3}(298 K)	Species	k_{NO3}(298 K)
METHANE	1D-18 [b]	TRANS-2-PENTENE	3.70D-13 [a]
ETHANE	1D-17 [b]	1-HEXENE	1.20D-14 [a]
PROPANE	7D-17 [b]	1-3 BUTADIENE	1.03D-13 [a]
N-BUTANE	4.6D-17 [b]	ISOPRENE	7.0D-13 [b]
I-BUTANE	1.1D-16 [b]	STYRENE	1.50D-12 [a]
ETHYLENE	2.1D-16 [b]	ETHYNE	1D-16 [b]
PROPYLENE	9.5D-15 [b]	BENZENE	3D-17 [b]
1-BUTENE	1.3D-14 [b]	TOLUENE	7.8D-17 [b]
CIS-2-BUTENE	3.50D-13 [a]	O-XYLENE	4.10D-16 [a]
TRANS-2-BUTENE	3.90D-13 [a]	M-XYLENE	2.60D-16 [a]
I-BUTENE	3.4D-13 [b]	P-XYLENE	5.00D-16 [a]
1-PENTENE	1.20D-14 [a]	ETHYL BENZENE	1.20D-16 [a]
CIS-2-PENTENE	3.70D-13 [a]	N-PROPYL BENZENE	1.40D-16 [a]

Note: a. MCM; b. IUPAC

Appendix B: Evaluations of box model method by ambient data.
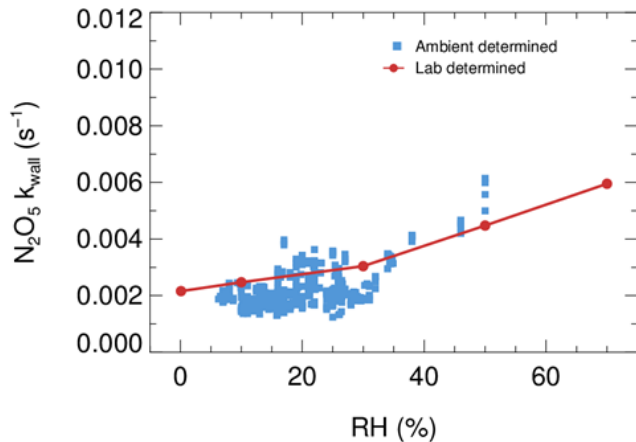
Figure B1. The derived dependence of N_2O_5 wall loss on RH at laboratory condition (red dots) and field measurement (blue square)
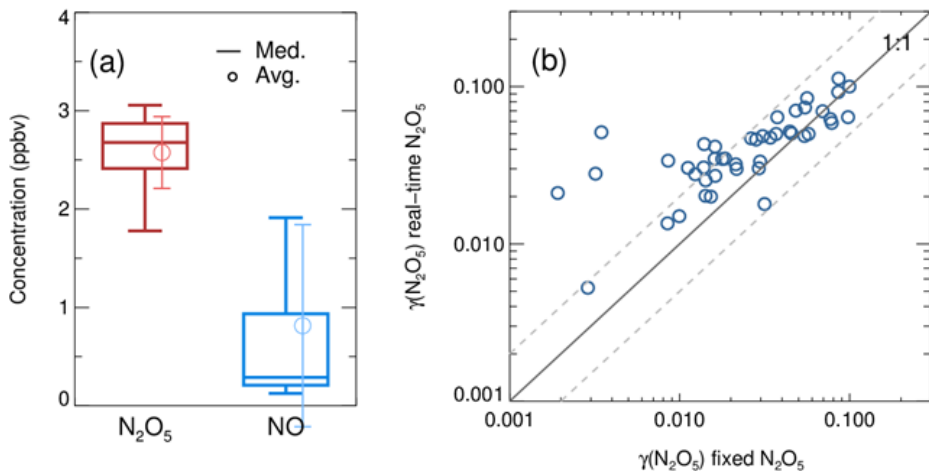
Figure B2. (a) the box whisker of N_2O_5 source and NO measured before the entrance; (b) the inter-comparison of derived N_2O_5 uptake coefficient by using a fixed initial N_2O_5 and a dynamic measured N_2O_5 at the flow tube entrance in the iterative box model.

718 **Author contributions.** K.D.L. and H.C.W. designed the study. X.R.C and H.C.W. analyzed

719 the data and wrote the paper with input from K.D.L.

720

732 **References**

733 Ahern, A. T., Goldberger, L., Jahl, L., Thornton, J., and Sullivan, R. C.: Production of N2O5 and ClNO2 through

734 Nocturnal Processing of Biomass-Burning Aerosol, Environmental Science & Technology, 52, 550-559,

735 10.1021/acs.est.7b04386, 2018.

736 Anttila, T., Kiendler-Scharr, A., Tillmann, R., and Mentel, T. F.: On the reactive uptake of gaseous compounds

737 by organic-coated aqueous aerosols: Theoretical analysis and application to the heterogeneous hydrolysis of

738 N2O5, J. Phys. Chem. A, 110, 10435-10443, 10.1021/jp062403c, 2006.

739 Baasandorj, M., Hoch, S. W., Bares, R., Lin, J. C., Brown, S. S., Millet, D. B., Martin, R., Kelly, K., Zarzana, K.

740 J., Whiteman, C. D., Dube, W. P., Tonnesen, G., Jaramillo, I. C., and Sohl, J.: Coupling between Chemical and

741 Meteorological Processes under Persistent Cold-Air Pool Conditions: Evolution of Wintertime PM2.5 Pollution

742 Events and N2O5 Observations in Utah's Salt Lake Valley, Environmental Science & Technology, 51, 5941-5950,

743 10.1021/acs.est.6b06603, 2017.

744 Badger, C. L., Griffiths, P. T., George, I., Abbatt, J. P. D., and Cox, R. A.: Reactive uptake of N2O5 by aerosol

745 particles containing mixtures of humic acid and ammonium sulfate, J. Phys. Chem. A, 110, 6986-6994,

746 10.1021/jp0562678, 2006.

747 Bertram, A. K., Martin, S. T., Hanna, S. J., Smith, M. L., Bodsworth, A., Chen, Q., Kuwata, M., Liu, A., You, Y.,
748 and Zorn, S. R.: Predicting the relative humidities of liquid-liquid phase separation, efflorescence, and
749 deliquescence of mixed particles of ammonium sulfate, organic material, and water using the organic-to-sulfate
750 mass ratio of the particle and the oxygen-to-carbon elemental ratio of the organic component, Atmos. Chem.
751 Phys., 11, 10995-11006, 10.5194/acp-11-10995-2011, 2011.

752 Bertram, T., and Thornton, J.: Toward a general parameterization of N 2 O 5 reactivity on aqueous particles: the
753 competing effects of particle liquid water, nitrate and chloride, Atmos. Chem. Phys., 9, 8351-8363, 2009a.

754 Bertram, T. H., and Thornton, J. A.: Toward a general parameterization of N2O5 reactivity on aqueous particles:
755 the competing effects of particle liquid water, nitrate and chloride, Atmos. Chem. Phys., 9, 8351-8363,
756 10.5194/acp-9-8351-2009, 2009b.

757 Bertram, T. H., Thornton, J. A., and Riedel, T. P.: An experimental technique for the direct measurement of N2O5
758 reactivity on ambient particles, Atmospheric Measurement Techniques, 2, 231-242, 10.5194/amt-2-231-2009,
759 2009a.

760 Bertram, T. H., Thornton, J. A., Riedel, T. P., Middlebrook, A. M., Bahreini, R., Bates, T. S., Quinn, P. K., and
761 Coffman, D. J.: Direct observations of N2O5 reactivity on ambient aerosol particles, Geophys. Res. Lett., 36,
762 10.1029/2009gl040248, 2009b.

763 Brown, S., Stark, H., Ciciora, S., McLaughlin, R., and Ravishankara, A. R.: Simultaneous in situ Detection of
764 Atmospheric NO3 and N2O5 via Cavity Ring-down Spectroscopy, Rev. Sci. Instrum., 73, 3291-3301,
765 10.1063/1.1499214, 2002.

766 Brown, S. S., Ryerson, T. B., Wollny, A. G., Brock, C. A., Peltier, R., Sullivan, A. P., Weber, R. J., Dube, W. P.,
767 Trainer, M., Meagher, J. F., Fehsenfeld, F. C., and Ravishankara, A. R.: Variability in nocturnal nitrogen oxide
768 processing and its role in regional air quality, Science, 311, 67-70, 10.1126/science.1120120, 2006.

769 Brown, S. S., Dube, W. P., Fuchs, H., Ryerson, T. B., Wollny, A. G., Brock, C. A., Bahreini, R., Middlebrook, A.
770 M., Neuman, J. A., Atlas, E., Roberts, J. M., Osthoff, H. D., Trainer, M., Fehsenfeld, F. C., and Ravishankara, A.
771 R.: Reactive uptake coefficients for N2O5 determined from aircraft measurements during the Second Texas Air
772 Quality Study: Comparison to current model parameterizations, J. Geophys. Res.- Atmos., 114, D00F10(01-16),
773 Artn D00f10
774 10.1029/2008jd011679, 2009.

775 Brown, S. S., and Stutz, J.: Nighttime radical observations and chemistry, Chem. Soc. Rev., 41, 6405-6447,
776 10.1039/c2cs35181a, 2012.

777 Brown, S. S., Dubé, W. P., Tham, Y. J., Zha, Q., Xue, L., Poon, S., Wang, Z., Blake, D. R., Tsui, W., Parrish, D.
778 D., and Wang, T.: Nighttime chemistry at a high altitude site above Hong Kong, J. Geophys. Res.: Atmos., 121,
779 2457-2475, 10.1002/2015jd024566, 2016.

780 Chang, W. L., Bhave, P. V., Brown, S. S., Riemer, N., Stutz, J., and Dabdub, D.: Heterogeneous atmospheric
781 chemistry, ambient measurements, and model calculations of N2O5: A review, Aerosol Sci. Technol., 45, 665-
782 695, 2011.

783 Chen, X., Wang, H., Lu, K., Li, C., Zhai, T., Tan, Z., Ma, X., Yang, X., Liu, Y., Chen, S., Dong, H., Li, X., Wu,
784 Z., Hu, M., Zeng, L., and Zhang, Y.: Field Determination of Nitrate Formation Pathway in Winter Beijing,
785 Environmental Science & Technology, 54, 9243-9253, 10.1021/acs.est.0c00972, 2020.

786 Chen, X., Wang, H., and Lu, K.: Interpretation of NO 3–N 2 O 5 observation via steady state in high aerosol air
787 mass: The impact of equilibrium coefficient in ambient conditions, Atmospheric Chemistry and Physics
788 Discussions, 1-14, 2021.

789 Cosman, L. M., Knopf, D. A., and Bertram, A. K.: N2O5 reactive uptake on aqueous sulfuric acid solutions

coated with branched and straight-chain insoluble organic surfactants, J. Phys. Chem. A, 112, 2386-2396, 10.1021/jp710685r, 2008.

Danckwerts, P. V.: Continuous flow systems: distribution of residence times, Chem. Eng. Sci., 2, 1-13, 1953.

Davis, J. M., Bhave, P. V., and Foley, K. M.: Parameterization of N2O5 reaction probabilities on the surface of particles containing ammonium, sulfate, and nitrate, Atmos. Chem. Phys., 8, 5295-5311, 10.5194/acp-8-5295-2008, 2008.

Dentener, F. J., and Crutzen, P. J.: Reaction Of N2O5 On Tropospheric Aerosols - Impact On The Global Distributions Of NOx, O3, And OH, Journal of Geophysical Research Atmospheres, 98, 7149-7163, 1993.

Escoreia, E. N., Sjostedt, S. J., and Abbatt, J. P. D.: Kinetics of N2O5 Hydrolysis on Secondary Organic Aerosol and Mixed Ammonium Bisulfate-Secondary Organic Aerosol Particles, J. Phys. Chem. A, 114, 13113-13121, 10.1021/jp107721v, 2010.

Evans, M., and Jacob, D. J.: Impact of new laboratory studies of N2O5 hydrolysis on global model budgets of tropospheric nitrogen oxides, ozone, and OH, Geophys. Res. Lett., 32, 2005.

Folkers, M., Mentel, T. F., and Wahner, A.: Influence of an organic coating on the reactivity of aqueous aerosols probed by the heterogeneous hydrolysis of N2O5, Geophys. Res. Lett., 30, Artn 1644
10.1029/2003gl017168, 2003.

Fried, A., Henry, B. E., Calvert, J. G., and Mozurkewich, M.: THE REACTION PROBABILITY OF N_2O_5 WITH SULFURIC-ACID AEROSOLS AT STRATOSPHERIC TEMPERATURES AND COMPOSITIONS, J. Geophys. Res.- Atmos., 99, 3517-3532, 10.1029/93jd01907, 1994.

Fu, X., Wang, T., Gao, J., Wang, P., Liu, Y., Wang, S., Zhao, B., and Xue, L.: Persistent Heavy Winter Nitrate Pollution Driven by Increased Photochemical Oxidants in Northern China, Environ. Sci. Technol., 54, 3881-3889, 10.1021/acs.est.9b07248, 2020.

Fuchs, N. A., and Sutugin, A. G.: Highly Dispersed Aerosol, Halsted Press, 1970.

Gaston, C. J., Thornton, J. A., and Ng, N. L.: Reactive uptake of N2O5 to internally mixed inorganic and organic particles: the role of organic carbon oxidation state and inferred organic phase separations, Atmos. Chem. Phys., 14, 5693-5707, 10.5194/acp-14-5693-2014, 2014.

Gaston, C. J., and Thornton, J. A.: Reacto-Diffusive Length of N2O5 in Aqueous Sulfate- and Chloride-Containing Aerosol Particles, J. Phys. Chem. A, 120, 1039-1045, 10.1021/acs.jpca.5b11914, 2016.

Griffiths, P. T., Badger, C. L., Cox, R. A., Folkers, M., Henk, H. H., and Mentel, T. F.: Reactive Uptake of N2O5 by Aerosols Containing Dicarboxylic Acids. Effect of Particle Phase, Composition, and Nitrate Content, J. Phys. Chem. A, 113, 5082-5090, 10.1021/jp8096814, 2009.

Gross, S., Iannone, R., Xiao, S., and Bertram, A. K.: Reactive uptake studies of NO3 and N2O5 on alkenoic acid, alkanoate, and polyalcohol substrates to probe nighttime aerosol chemistry, PCCP, 11, 7792-7803, 10.1039/b904741g, 2009.

Hallquist, M., Stewart, D. J., Baker, J., and Cox, R. A.: Hydrolysis of N_2O_5 on submicron sulfuric acid aerosols, J. Phys. Chem. A, 104, 3984-3990, 10.1021/jp9939625, 2000.

Hallquist, M., Stewart, D. J., Stephenson, S. K., and Anthony Cox, R.: Hydrolysis of N_2O_5 on sub-micron sulfate aerosols, PCCP, 5, 3453, 10.1039/b301827j, 2003.

Hu, J. H., and Abbatt, J. P. D.: Reaction probabilities for N2O5 hydrolysis on sulfuric acid and ammonium sulfate aerosols at room temperature, J. Phys. Chem. A, 101, 871-878, DOI 10.1021/jp9627436, 1997.

Huang, Y., Coggon, M., Zhao, R., Lignell, H., Bauer, M., Flagan, R., and Seinfeld, J.: The Caltech Photooxidation Flow Tube reactor: Design, fluid dynamics and characterization, Atmospheric Measurement Techniques, 10, 839-867, 10.5194/amt-10-839-2017, 2017.

Kane, S. M., Caloz, F., and Leu, M. T.: Heterogeneous uptake of gaseous N_2O_5 by $(NH_4)_2SO_4$, NH_4HSO_4, and H_2SO_4 aerosols, J. Phys. Chem. A, 105, 6465-6470, 10.1021/jp010490x, 2001.

Karagulian, F., Santschi, C., and Rossi, M.: The heterogeneous chemical kinetics of N_2O_5 on $CaCO_3$ and other atmospheric mineral dust surrogates, Atmos. Chem. Phys., 6, 1373-1388, 2006.

Lambe, A., Ahern, A., Williams, L., Slowik, J., Wong, J., Abbatt, J., Brune, W., Ng, N., Wright, J., and Croasdale, D.: Characterization of aerosol photooxidation flow reactors: heterogeneous oxidation, secondary organic aerosol formation and cloud condensation nuclei activity measurements, Atmospheric Measurement Techniques, 4, 445-461, 2011.

Li, C. M., Wang, H. C., Chen, X. R., Zhai, T. Y., Chen, S. Y., Li, X., Zeng, L. M., and Lu, K. D.: Thermal dissociation cavity-enhanced absorption spectrometer for measuring NO2, RO2NO2, and RONO2 in the atmosphere, Atmospheric Measurement Techniques, 14, 4033-4051, 10.5194/amt-14-4033-2021, 2021.

Li, Q., Zhang, L., Wang, T., Tham, Y. J., Ahmadov, R., Xue, L., Zhang, Q., and Zheng, J.: Impacts of heterogeneous uptake of dinitrogen pentoxide and chlorine activation on ozone and reactive nitrogen partitioning: improvement and application of the WRF-Chem model in southern China, Atmos. Chem. Phys., 16, 14875-14890, 10.5194/acp-16-14875-2016, 2016.

Liu, X., Gu, J., Li, Y., Cheng, Y., Qu, Y., Han, T., Wang, J., Tian, H., Chen, J., and Zhang, Y.: Increase of aerosol scattering by hygroscopic growth: Observation, modeling, and implications on visibility, Atmos. Res. , 132, 91-101, 2013.

Lowe, D., Archer-Nicholls, S., Morgan, W., Allan, J., Utembe, S., Ouyang, B., Aruffo, E., Le Breton, M., Zaveri, R. A., and Di Carlo, P.: WRF-Chem model predictions of the regional impacts of N_2O_5 heterogeneous processes on night-time chemistry over north-western Europe, Atmos. Chem. Phys., 15, 1385-1409, 2015.

Macintyre, H., and Evans, M.: Sensitivity of a global model to the uptake of N_2O_5 by tropospheric aerosol, Atmos. Chem. Phys., 10, 7409-7414, 2010.

Martin, S. T.: Phase transitions of aqueous atmospheric particles, Chem. Rev., 100, 3403-3454, 2000.

McDuffie, E. E., Fibiger, D. L., Dubé, W. P., Lopez-Hilfiker, F., Lee, B. H., Thornton, J. A., Shah, V., Jaeglé, L., Guo, H., Weber, R. J., Michael Reeves, J., Weinheimer, A. J., Schroder, J. C., Campuzano-Jost, P., Jimenez, J. L., Dibb, J. E., Veres, P., Ebben, C., Sparks, T. L., Wooldridge, P. J., Cohen, R. C., Hornbrook, R. S., Apel, E. C., Campos, T., Hall, S. R., Ullmann, K., and Brown, S. S.: Heterogeneous N_2O_5 Uptake During Winter: Aircraft Measurements During the 2015 WINTER Campaign and Critical Evaluation of Current Parameterizations, J. Geophys. Res.: Atmos., 123, 4345-4372, 10.1002/2018jd028336, 2018.

McDuffie, E. E., Womack, C. C., Fibiger, D. L., Dube, W. P., Franchin, A., Middlebrook, A. M., Goldberger, L., Lee, B. H., Thornton, J. A., Moravek, A., Murphy, J. G., Baasandorj, M., and Brown, S. S.: On the contribution of nocturnal heterogeneous reactive nitrogen chemistry to particulate matter formation during wintertime pollution events in Northern Utah, Atmos. Chem. Phys., 19, 9287-9308, 10.5194/acp-19-9287-2019, 2019.

McNeill, V. F., Patterson, J., Wolfe, G. M., and Thornton, J. A.: The effect of varying levels of surfactant on the reactive uptake of N2O5 to aqueous aerosol, Atmos. Chem. Phys., 6, 1635-1644, 10.5194/acp-6-1635-2006, 2006.

Mentel, T. F., Sohn, M., and Wahner, A.: Nitrate effect in the heterogeneous hydrolysis of dinitrogen pentoxide on aqueous aerosols, PCCP, 1, 5451-5457, 10.1039/a905338g, 1999.

Mielke, L. H., Stutz, J., Tsai, C., Hurlock, S. C., Roberts, J. M., Veres, P. R., Froyd, K. D., Hayes, P. L., Cubison, M. J., Jimenez, J. L., Washenfelder, R. A., Young, C. J., Gilman, J. B., de Gouw, J. A., Flynn, J. H., Grossberg, N., Lefer, B. L., Liu, J., Weber, R. J., and Osthoff, H. D.: Heterogeneous formation of nitryl chloride and its role as a nocturnal NOx reservoir species during CalNex-LA 2010, J. Geophys. Res.: Atmos., 118, 10,638-610,652, 10.1002/jgrd.50783, 2013.

876 Mitroo, D., Gill, T. E., Haas, S., Pratt, K. A., and Gaston, C. J.: ClNO2 Production from N2O5 Uptake on Saline

877 Playa Dusts: New Insights into Potential Inland Sources of ClNO2, Environmental Science & Technology, 53,

878 7442-7452, 10.1021/acs.est.9b01112, 2019.

879 Mozurkewich, M., and Calvert, J. G.: REACTION PROBABILITY OF N2O5 ON AQUEOUS AEROSOLS, J.

880 Geophys. Res.- Atmos., 93, 15889-15896, 10.1029/JD093iD12p15889, 1988.

881 Murray, L. T., Fiore, A. M., Shindell, D. T., Naik, V., and Horowitz, L. W.: Large uncertainties in global hydroxyl

882 projections tied to fate of reactive nitrogen and carbon, Proceedings of the National Academy of Sciences, 118,

883 2021.

884 Osthoff, H. D., Roberts, J. M., Ravishankara, A. R., Williams, E. J., Lerner, B. M., Sommariva, R., Bates, T. S.,

885 Coffman, D., Quinn, P. K., Dibb, J. E., Stark, H., Burkholder, J. B., Talukdar, R. K., Meagher, J., Fehsenfeld, F.

886 C., and Brown, S. S.: High levels of nitryl chloride in the polluted subtropical marine boundary layer, Nat.

887 Geosci. , 1, 324-328, 10.1038/ngeo177, 2008.

888 Phillips, G. J., Thieser, J., Tang, M., Sobanski, N., Schuster, G., Fachinger, J., Drewnick, F., Borrmann, S.,

889 Bingemer, H., Lelieveld, J., and Crowley, J. N.: Estimating N_2O_5 uptake coefficients using ambient measurements

890 of NO_3, N_2O_5, $ClNO_2$ and particle-phase nitrate, Atmos. Chem. Phys., 16, 13231-13249, 10.5194/acp-16-13231-

891 2016, 2016.

892 Platt, U. F., Winer, A. M., Biermann, H. W., Atkinson, R., and Pitts, J. N.: Measurement of nitrate radical

893 concentrations in continental air, Environmental Science & Technology, 18, 365-369, 10.1021/es00123a015,

894 1984.

895 Prabhakar, G., Parworth, C. L., Zhang, X. L., Kim, H., Young, D. E., Beyersdorf, A. J., Ziemba, L. D., Nowak,

896 J. B., Bertram, T. H., Faloona, I. C., Zhang, Q., and Cappa, C. D.: Observational assessment of the role of

897 nocturnal residual-layer chemistry in determining daytime surface particulate nitrate concentrations, Atmos.

898 Chem. Phys., 17, 14747-14770, 10.5194/acp-17-14747-2017, 2017.

899 Riedel, T. P., Bertram, T. H., Crisp, T. A., Williams, E. J., Lerner, B. M., Vlasenko, A., Li, S. M., Gilman, J., de

900 Gouw, J., Bon, D. M., Wagner, N. L., Brown, S. S., and Thornton, J. A.: Nitryl Chloride and Molecular Chlorine

901 in the Coastal Marine Boundary Layer, Environmental Science & Technology, 46, 10463-10470,

902 10.1021/es204632r, 2012a.

903 Riedel, T. P., Bertram, T. H., Ryder, O. S., Liu, S., Day, D. A., Russell, L. M., Gaston, C. J., Prather, K. A., and

904 Thornton, J. A.: Direct N_2O_5 reactivity measurements at a polluted coastal site, Atmos. Chem. Phys., 12, 2959-

905 2968, 10.5194/acp-12-2959-2012, 2012b.

906 Riedel, T. P., Wagner, N. L., Dube, W. P., Middlebrook, A. M., Young, C. J., Ozturk, F., Bahreini, R., VandenBoer,

907 T. C., Wolfe, D. E., Williams, E. J., Roberts, J. M., Brown, S. S., and Thornton, J. A.: Chlorine activation within

908 urban or power plant plumes: Vertically resolved ClNO2 and Cl-2 measurements from a tall tower in a polluted

909 continental setting, J. Geophys. Res.- Atmos., 118, 8702-8715, 10.1002/jgrd.50637, 2013.

910 Riemer, N., Vogel, H., Vogel, B., Schell, B., Ackermann, I., Kessler, C., and Hass, H.: Impact of the heterogeneous

911 hydrolysis of N2O5 on chemistry and nitrate aerosol formation in the lower troposphere under photosmog

912 conditions, J. Geophys. Res.- Atmos., 108, 10.1029/2002jd002436, 2003.

913 Riemer, N., Vogel, H., Vogel, B., Anttila, T., Kiendler-Scharr, A., and Mentel, T. F.: Relative importance of

914 organic coatings for the heterogeneous hydrolysis of N2O5during summer in Europe, J. Geophys. Res. , 114,

915 10.1029/2008jd011369, 2009.

916 Royer, H. M., Mitroo, D., Hayes, S. M., Haas, S. M., Pratt, K. A., Blackwelder, P. L., Gill, T. E., and Gaston, C.

917 J.: The Role of Hydrates, Competing Chemical Constituents, and Surface Composition on ClNO2 Formation,

918 Environmental Science & Technology, 55, 2869-2877, 10.1021/acs.est.0c06067, 2021.

Sarwar, G., Simon, H., Bhave, P., and Yarwood, G.: Examining the impact of heterogeneous nitryl chloride production on air quality across the United States, Atmospheric Chemistry & Physics, 12, 6455-6473, 10.5194/acp-12-6455-2012, 2012.

Schweitzer, F., Mirabel, P., and George, C.: Multiphase chemistry of N2O5, ClNO2, and BrNO2, The Journal of Physical Chemistry A, 102, 3942-3952, 1998.

Tang, M., Telford, P., Pope, F. D., Rkiouak, L., Abraham, N., Archibald, A. T., Braesicke, P., Pyle, J., McGregor, J., and Watson, I.: Heterogeneous reaction of N 2 O 5 with airborne TiO 2 particles and its implication for stratospheric particle injection, Atmos. Chem. Phys., 14, 6035-6048, 2014.

Tham, Y. J., Wang, Z., Li, Q. Y., Yun, H., Wang, W. H., Wang, X. F., Xue, L. K., Lu, K. D., Ma, N., Bohn, B., Li, X., Kecorius, S., Gross, J., Shao, M., Wiedensohler, A., Zhang, Y. H., and Wang, T.: Significant concentrations of nitryl chloride sustained in the morning: investigations of the causes and impacts on ozone production in a polluted region of northern China, Atmos. Chem. Phys., 16, 14959-14977, 10.5194/acp-16-14959-2016, 2016.

Tham, Y. J., Wang, Z., Li, Q. Y., Wang, W. H., Wang, X. F., Lu, K. D., Ma, N., Yan, C., Kecorius, S., Wiedensohler, A., Zhang, Y. H., and Wang, T.: Heterogeneous N2O5 uptake coefficient and production yield of ClNO2 in polluted northern China: roles of aerosol water content and chemical composition, Atmos. Chem. Phys., 18, 13155-13171, 10.5194/acp-18-13155-2018, 2018.

Thornton, J. A., Braban, C. F., and Abbatt, J. P. D.: N2O5 hydrolysis on sub-micron organic aerosols: the effect of relative humidity, particle phase, and particle size, PCCP, 5, 4593, 10.1039/b307498f, 2003.

Thornton, J. A., and Abbatt, J. P. D.: N2O5 reaction on submicron sea salt aerosol: Kinetics, products, and the effect of surface active organics, J. Phys. Chem. A, 109, 10004-10012, 10.1021/jp054183t, 2005.

Thornton, J. A., Kercher, J. P., Riedel, T. P., Wagner, N. L., Cozic, J., Holloway, J. S., Dube, W. P., Wolfe, G. M., Quinn, P. K., Middlebrook, A. M., Alexander, B., and Brown, S. S.: A large atomic chlorine source inferred from mid-continental reactive nitrogen chemistry, Nature, 464, 271-274, 10.1038/nature08905, 2010.

Van Doren, J. M., Watson, L. R., Davidovits, P., Worsnop, D. R., Zahniser, M. S., and Kolb, C. E.: Temperature dependence of the uptake coefficients of nitric acid, hydrochloric acid and nitrogen oxide (N2O5) by water droplets, J. Phys. Chem., 94, 3265-3269, 1990.

Wagner, N. L., Riedel, T. P., Young, C. J., Bahreini, R., Brock, C. A., Dubé, W. P., Kim, S., Middlebrook, A. M., Öztürk, F., Roberts, J. M., Russo, R., Sive, B., Swarthout, R., Thornton, J. A., VandenBoer, T. C., Zhou, Y., and Brown, S. S.: N2O5 uptake coefficients and nocturnal NO2 removal rates determined from ambient wintertime measurements, J. Geophys. Res.: Atmos., 118, 9331-9350, 10.1002/jgrd.50653, 2013.

Wahner, A., Mentel, T. F., Sohn, M., and Stier, J.: Heterogeneous reaction of N2O5 on sodium nitrate aerosol, J. Geophys. Res.: Atmos., 103, 31103-31112, 10.1029/1998jd100022, 1998.

Wang, H., Chen, J., and Lu, K.: Development of a portable cavity-enhanced absorption spectrometer for the measurement of ambient NO_3 and N_2O_5: experimental setup, lab characterizations, and field applications in a polluted urban environment, Atmospheric Measurement Techniques, 10, 1465-1479, 10.5194/amt-10-1465-2017, 2017a.

Wang, H., Lu, K., Chen, X., Zhu, Q., Chen, Q., Guo, S., Jiang, M., Li, X., Shang, D., Tan, Z., Wu, Y., Wu, Z., Zou, Q., Zheng, Y., Zeng, L., Zhu, T., Hu, M., and Zhang, Y.: High N_2O_5 Concentrations Observed in Urban Beijing: Implications of a Large Nitrate Formation Pathway, Environ Sci Tech Let, 4, 416-420, 10.1021/acs.estlett.7b00341, 2017b.

Wang, H., Chen, X., Lu, K., Tan, Z., Ma, X., Wu, Z., Li, X., Liu, Y., Shang, D., Wu, Y., Zeng, L., Hu, M., Schmitt, S., Kiendler-Scharr, A., Wahner, A., and Zhang, Y.: Wintertime N2O5 uptake coefficients over the North China

962 Plain, Science Bulletin, 65, 765-774, https://doi.org/10.1016/j.scib.2020.02.006, 2020a.

963 Wang, H. C., Lu, K. D., Chen, X. R., Zhu, Q. D., Chen, Q., Guo, S., Jiang, M. Q., Li, X., Shang, D. J., Tan, Z. F.,
964 Wu, Y. S., Wu, Z. J., Zou, Q., Zheng, Y., Zeng, L. M., Zhu, T., Hu, M., and Zhang, Y. H.: High N2O5
965 Concentrations Observed in Urban Beijing: Implications of a Large Nitrate Formation Pathway, Environ Sci Tech
966 Let, 4, 416-420, 10.1021/acs.estlett.7b00341, 2017c.

967 Wang, H. C., Lu, K. D., Chen, X. R., Zhu, Q. D., Wu, Z. J., Wu, Y. S., and Sun, K.: Fast particulate nitrate
968 formation via N2O5 uptake aloft in winter in Beijing, Atmos. Chem. Phys., 18, 10483-10495, 10.5194/acp-18-
969 10483-2018, 2018a.

970 Wang, H. C., Lu, K. D., Guo, S., Wu, Z. J., Shang, D. J., Tan, Z. F., Wang, Y. J., Le Breton, M., Lou, S. R., Tang,
971 M. J., Wu, Y. S., Zhu, W. F., Zheng, J., Zeng, L. M., Hallquist, M., Hu, M., and Zhang, Y. H.: Efficient N2O5
972 uptake and NO3 oxidation in the outflow of urban Beijing, Atmos. Chem. Phys., 18, 9705-9721, 10.5194/acp-
973 18-9705-2018, 2018b.

974 Wang, H. C., Chen, X. R., Lu, K. D., Hu, R. Z., Li, Z. Y., Wang, H. L., Ma, X. F., Yang, X. P., Chen, S. Y., Dong,
975 H. B., Liu, Y., Fang, X., Zeng, L. M., Hu, M., and Zhang, Y. H.: NO3 and N2O5 chemistry at a suburban site
976 during the EXPLORE-YRD campaign in 2018, Atmos. Environ., 224, ARTN 117180
977 10.1016/j.atmosenv.2019.117180, 2020b.

978 Wang, H. C., Peng, C., Wang, X., Lou, S. R., Lu, K. D., Gan, G. C., Jia, X. H., Chen, X. R., Chen, J., Wang, H.
979 L., Fan, S. J., Wang, X. M., and Tang, M. J.: N2O5 uptake onto saline mineral dust: a potential missing source of
980 tropospheric ClNO2 in inland China, Atmos. Chem. Phys., 22, 1845-1859, 10.5194/acp-22-1845-2022, 2022.

981 Wang, W., Wang, Z., Yu, C., Xia, M., Peng, X., Zhou, Y., Yue, D., Ou, Y., and Wang, T.: An in situ flow tube
982 system for direct measurement of N2O5 heterogeneous uptake coefficients in polluted environments,
983 Atmospheric Measurement Techniques, 11, 5643-5655, 10.5194/amt-11-5643-2018, 2018c.

984 Wang, X., Wang, H., Xue, L., Wang, T., Wang, L., Gu, R., Wang, W., Tham, Y. J., Wang, Z., Yang, L., Chen, J.,
985 and Wang, W.: Observations of N_2O_5 and $ClNO_2$ at a polluted urban surface site in North China: High N_2O_5
986 uptake coefficients and low $ClNO_2$ product yields, Atmos. Environ., 156, 125-134,
987 10.1016/j.atmosenv.2017.02.035, 2017d.

988 Wang, Y. L., Song, W., Yang, W., Sun, X. C., Tong, Y. D., Wang, X. M., Liu, C. Q., Bai, Z. P., and Liu, X. Y.:
989 Influences of atmospheric pollution on the contributions of major oxidation pathways to PM2. 5 nitrate formation
990 in Beijing, J. Geophys. Res.: Atmos., 124, 4174-4185, 2019.

991 Wang, Z., Wang, W., Tham, Y. J., Li, Q., Wang, H., Wen, L., Wang, X., and Wang, T.: Fast heterogeneous N2O5
992 uptake and ClNO2 production in power plant and industrial plumes observed in the nocturnal residual layer over
993 the North China Plain, Atmos. Chem. Phys., 17, 12361-12378, 10.5194/acp-17-12361-2017, 2017e.

994 Wang, Z., Wang, W. H., Tham, Y. J., Li, Q. Y., Wang, H., Wen, L., Wang, X. F., and Wang, T.: Fast heterogeneous
995 N2O5 uptake and ClNO2 production in power plant and industrial plumes observed in the nocturnal residual
996 layer over the North China Plain, Atmos. Chem. Phys., 17, 12361-12378, 10.5194/acp-17-12361-2017, 2017f.

997 Wu, C., Zhang, S., Wang, G., Lv, S., Li, D., Liu, L., Li, J., Liu, S., Du, W., and Meng, J.: Efficient heterogeneous
998 formation of ammonium nitrate on the saline mineral particle surface in the atmosphere of East Asia during dust
999 storm periods, Environmental Science & Technology, 54, 15622-15630, 2020.

1000 Xia, M., Wang, W., Wang, Z., Gao, J., Li, H., Liang, Y., Yu, C., Zhang, Y., Wang, P., Zhang, Y., Bi, F., Cheng, X.,
1001 and Tao, W.: Heterogeneous Uptake of N2O5 in Sand Dust and Urban Aerosols Observed during the Dry Season
1002 in Beijing, Atmosphere, 10, 204, 10.3390/atmos10040204, 2019.

1003 Yu, C., Wang, Z., Xia, M., Fu, X., Wang, W., Yee Jun, T., Chen, T., Zheng, P., Li, H., Shan, Y., Wang, X., Xue,
1004 L., Zhou, Y., Yue, D., Ou, Y., Gao, J., Lu, K., Brown, S., Zhang, Y., and Tao, W.: Heterogeneous N_2O_5 reactions

1005   on atmospheric aerosols at four Chinese sites: improving model representation of uptake parameters, Atmos.

1006   Chem. Phys., 20, 4367-4378, 10.5194/acp-20-4367-2020, 2020a.

1007   Yu, C., Wang, Z., Xia, M., Fu, X., Wang, W. H., Tham, Y. J., Chen, T. S., Zheng, P. G., Li, H. Y., Shan, Y., Wang,

1008   X. F., Xue, L. K., Zhou, Y., Yue, D. L., Ou, Y. B., Gao, J., Lu, K. D., Brown, S. S., Zhang, Y. H., and Wang, T.:

1009   Heterogeneous N2O5 reactions on atmospheric aerosols at four Chinese sites: improving model representation

1010   of uptake parameters, Atmos. Chem. Phys., 20, 4367-4378, 10.5194/acp-20-4367-2020, 2020b.

1011   Yun, H., Wang, T., Wang, W. H., Tham, Y. J., Li, Q. Y., Wang, Z., and Poon, S. C. N.: Nighttime NOx loss and

1012   ClNO2 formation in the residual layer of a polluted region: Insights from field measurements and an iterative

1013   box model, Sci. Total Environ., 622, 727-734, 10.1016/j.scitotenv.2017.11.352, 2018.

1014